ANNEALING INDUCED EFFECTS ON PHYSICAL PROPERTIES OF $Co_{0.5}Zn_{0.5}Fe_2O_4$ NANOPARTICLES

By

MUBASHER

Department of Physics
Faculty of Basic and Applied Sciences
International Islamic University, Islamabad

(2012)

International Islamic Univ.
CENTRAL LIBRARY ISLAMABAD.

Accession No TH-9495

MS
620.5
MUA

-1 Nanotechnology

DATA ENTERED
04/3/13

ANNEALING INDUCED EFFECTS ON PHYSICAL PROPERTIES OF $Co_{0.5}Zn_{0.5}Fe_2O_4$ NANOPARTICLES

Researcher

Mubasher
(25-FBAS/MSPHY/F10)

Supervisor

Dr. Javed Iqbal
Assistant Professor,
Department of Physics, FBAS, IIUI

Department of Physics
Faculty of Basic and Applied Sciences
International Islamic University, Islamabad

(2012)

INTERNATIONAL ISLAMIC UNIVERSITY, ISLAMABAD

FACULTY OF BASIC AND APPLIED SCIENCES

DEPARTMENT OF PHYSICS

Dated: August 06, 2012

FINAL APPROVAL

It is certificate that we have read this dissertation entitled "**ANNEALING INDUCED EFFECTS ON PHYSICAL PROPERTIES OF $Co_{0.5}Zn_{0.5}Fe_2O_4$ NANOPARTICLES**" submitted by "**Mr. MUBASHER**" and it is our judgment that this project is of sufficient standard in scope and quality to warrant its acceptance by the International Islamic University, Islamabad for the MS Degree in Physics.

COMMITTEE

External Examiner

Internal Examiner
Dr. Naeem Ahmad
Assistant Professor
Department of Physics
International Islamic University, Islamabad.

Supervisor
Dr. Javed Iqbal
Assistant Professor
Department of Physics
International Islamic University, Islamabad.

Co-Supervisor
Dr.Ishaq Ahmad
Manager
National Centre for Physics
Quaid-i-Azam University, Islamabad.

INTERNATIONAL ISLAMIC UNIVERSITY, ISLAMABAD
FACULTY OF BASIC AND APPLIED SCIENCES
DEPARTMENT OF PHYSICS

ANNEALING INDUCED EFFECTS ON PHYSICAL PROPERTIES OF $Co_{0.5}Zn_{0.5}Fe_2O_4$ NANOPARTICLES

By

MUBASHER

(Registration No. 25-FBAS/MSPHY/F10)

A thesis submitted to

Department of Physics

for the award of the degree of

MS Physics

Signature: _____

(Chairman, Department of Physics)

Signature: _____

(Dean FBAS, IIU, Islamabad)

This work is submitted to Department of Physics,
International Islamic University, Islamabad
as a dissertation in partial fulfillment of
the requirement for the degree of
Master of Science in **Physics**.

O, GOD, OPEN OUR EYES,
TO SEE WHAT IS BEAUTIFUL,
OUR MINDS TO KNOW WHAT IS TRUE,
OUR HEARTS TO LOVE WHAT IS GOOD

DEDICATED TO:

My Loving Parents

DECLARATION

I hereby declare that this thesis work, neither as a whole nor a part of it has been copied out from any source. Further, work presented in this dissertation has not been submitted in support of any application for any other degree or qualification to any other university or institute.

Date: _____

MUBASHER

(25-FBAS/MSPHY/F10)

AKNOWLEDGEMENT

I am nothing but Alhamdulillah; **ALMIGHTY ALLAH** enabled me able to finish this project successfully. All praises and respects are for **HOLY PROPHET MUHAMMAD (SALLALLAHO-ALAIHE-WASALLAM)**, who is a source of guidance and knowledge for us.

I would like to thank to Chairman Department of Physics and Dean Faculty of Basic and Applied Sciences, IIUI for their cooperation during my research work.

I sincerely appreciate my supervisor, Dr. Javed Iqbal Saggu, for his encouragement, guidance, training, valuable suggestions, co-operation, continuous encouragements and guidance and personal interest. I am whole heartedly thankful for his patience and discussions throughout my research work.

I am thankful to Prof. Dr. Asghari Maqsood, School of Chemical and Materials Engineering, NUST, Islamabad, for providing me the opportunity to work in her lab. I would like to thank Mr. Shams-ud-din for his guidance in characterization of samples at SCME, NUST. I would also like to thank Mr. Tariq Jan, PhD scholar in my lab, for his personal interest in my research work. I would like to show my deep gratitude to Zunaira Tariq, Mr. Shakaib Arslan and Mr. Rizwan for friendly discussion and assistance during my research work.

I owe my deepest gratitude to my family especially my sisters for their prayers and affectionate behavior for my success.

Lastly, I oblige my special thanks to my brother Mr. Farrukh Shahzad Rajpoot for his encouragement and financial support which enabled me to complete this project.

Mubasher

PREFACE

The work presented in this thesis was carried out at the Nanoscience and Nanotechnology Laboratory, Department of Physics, Faculty of Basic and Applied Sciences, International Islamic University, Islamabad, Pakistan. The thesis is divided into four chapters. First chapter gives a brief introduction and literature survey of ferrites. Chapter two consists of experimental techniques of samples for investigation. Chapter three discusses the fabrication and preparation of the samples. Chapter four describes the effects of annealing on physical, magnetic and optical properties and characterization of Co-Zn ferrite nanoparticles. At the end, there is an overall conclusion of the thesis. References to the literature are mentioned at the end after conclusion.

ABSTRACT

The nanoparticles of Cobalt Zinc ferrites have been synthesized using Co-precipitation method. The size of nanoparticles has been controlled by optimizing different synthesis parameters such as pH value, reaction time and concentration of dopants. The Zinc ferrite nanoparticles have been doped with Cobalt in ratio. In order to enhance the physical properties, the prepared samples of $Co_{0.5}Zn_{0.5}Fe_2O_4$ have been annealed at 500°C, 650°C and 1000°C and then compared with as prepared sample. The single phase crystallinity and the evaluation of crystallite size of fine precipitated particles have been investigated by X-Ray Diffraction (XRD). The morphology of samples has been checked using Scanning Electron Microscopy (SEM). The prepared samples have nanoparticles shape and their size has been found increasing with the increase in annealing temperature. The composition of $Co_{1-x}Zn_xFe_2O_4$ ($x = 0.5$) have been determined using X-Ray Fluorescence (XRF) at room temperature. The presence of contents in the synthesized $Co_{1-x}Zn_xFe_2O_4$ ($x = 0.5$) has been checked using Energy-Dispersive X-ray Spectroscopy (EDX). The $Co_{1-x}Zn_xFe_2O_4$ ($x = 0.5$) ferrite nanoparticles have shown remarkable enhancement in magnetic moments; which have been investigated using Vibrating Sample Magnetometer (VSM). The band gap of $Co_{1-x}Zn_xFe_2O_4$ ($x = 0.5$) ferrite nanoparticles have been measured via UV Spectrometer and are found to be decreasing with the increase of annealing temperatures. The observed characteristics of Cobalt Zinc ferrite nanoparticles as a function of annealing temperature are the rising contender for many data storage and nanodevice applications.

TABLE OF CONTENTS

LIST OF FIGURES

LIST OF TABLES

LIST OF ABBREVIATIONS

NPs:	Nanoparticles
SEM:	Scanning Electron Microscope
XRD:	X-Ray Diffraction
EDX:	Energy Dispersive X-Ray Spectroscopy
XRF:	X-Ray Florescence
VSM:	Vibrating Sample Magnetometer
MS:	Magnetostatic Energy
FCC:	Face Centered Cube
Vis/NIR:	Visible and Near Infrared
Emu:	Electromagnetic Unit
UV:	Ultraviolet
Emf:	Electromotive Force
E_g:	Energy Band Gap
T_c:	Curie Temperature
T_N:	Neel Temperature

LIST OF SYMBOLS

χ:	Susceptibility
λ:	Wavelength
ρ:	Density
α:	Direction Cosines
Å:	Angstrom
τ:	Relaxation Time
μ:	Magnetic Dipole Moment
α^2:	Absorption coefficient
k:	Anisotropy Constant
□:	Viscosity of liquid carrier
τ_B:	Brownian Rotational Diffused Time

CHAPTER 1 - INTRODUCTION AND LITERATURE SURVEY

1.1 Introduction to Nanotechnology

Nanotechnology is one of the exciting and fastest growing areas in science, technology and engineering now-a-days. The convergence of several branches of science, i.e. material science, physics and chemistry gives arise to the functional systems of nanoscale dimensions of the order of one billionth of a meter. Ancient people while making glass have been unknowingly playing with materials on nanoscale. Modern era of nanoscience and nanotechnology started some fifty years ago when in December 1959 Nobel laureate Richard Feynman put forward the challenge by stating: **"There is plenty of rooms at the bottom"**. According to Professor Norio Taniguchi, term "nanotechnology" is basically the deformation, consolidation and process of separation of specimen by an atom or molecules. Dr. K. Eric Drexler explored the ideology of the physical phenomenon at nano scales and expressed them in his book "Engines of Creation and The Coming Era of Nanotechnology". In early 80s, the birth of cluster science gave spark in the field of science at nanoscale. Later on, the study of semiconductor nanocrystals opens the door for rapid increase in the number of quantum dots, metallic oxides and metallic nanoparticles.

Nanometer is abbreviated as nm that is the unit of length and it is 10^{-9} part of a meter. The human hair has diameter approximately 60-80,000 nanometers, while the length of ten hydrogen atoms placed in a row would approximately equal to 1nm. A material is said to be in nano-material if its size is below than 100 nm which leads to the significantly changes in its physical and chemical properties. For example, metallic gold has melting temperature of 1000 ^{o}C and it drops to 330 ^{o}C when its size reduces to 2 nm. It is observed that the aspect ratio (surface to volume ratio) will be large when the size of particle is small. For instance, the grain surface of a gram of gold is extremely valuable when size is <100 nm. As the surface atoms are highly instable and active in a chemical reaction, this results an enhancement in chemical reaction, catalytic and surface absorption ability of the material.

Due to the various potential applications, the field of nanoscience is of deep interest besides the fundamental science. Roughly speaking, nano electronics (transistors, diodes etc.), nano material science (ferrites, ceramics etc.), nano biology (DNA, MRI etc.) and nano medicine (drug delivery) have spark applications at nanoscale. This opens the doors for tailoring the properties by

careful synthesis of the building blocks and their assembly to fabricate functional materials with improved properties. The current work and concept also cover these points, which are more advanced and up-to-date.

1.2 Nanoparticles

Spherical particles having diameter less than 100 nm are termed as nanoparticles. The particles whose size are in the range between 100 - 2500 nm and between 1 - 100 nm are termed as fine and ultrafine particles, respectively. Similarly, the nanoparticles cover range of 1 - 100 nm. Nanoparticles sometimes exhibit size related properties and sometimes they do not [1]; which differ significantly from bulk materials or fine particles. Many new nanocomposite materials with enriched properties can be fabricated by controlling the shape, composition and size of the nanoparticles. By the inclusion of selected nanoparticles, metals can be made stiff, strong and hard. As ceramics can have enhanced hardness and toughness, therefore, for the conduction of heat and electricity the insulating materials can be fabricated. Nanoparticles attain numerous characteristics such as monosized distribution or uniform size distribution, shape, morphology, chemical composition, redispersible and crystal structure among different particles.

1.3 Magnetic Overview

Magnetism is the primitive aspect of solid state physics which has been familiar to man as early as 800 B.C. Magnes in 900 B.C. documented one of the first encounters about magnetic material [2]. Dr. William Gilbert evolved modern concepts of magnetism and documented that the entire world is a big magnet by his systematically studied [3]. Since then, numerous contributions have helped to evolve modern theories about magnetism. Actually, the experimental discoveries lead towards the known magnetic properties of materials. The circular motion of charges inside atoms originates magnetic field in materials. The current passing through an electric wire produces a magnetic field around itself. A current loop surrounding an area "πr^2_{loop}" , carrying a current 'i', form magnetic dipole moment 'μ' with magnitude "$i\pi r^2_{loop}$" having electromagnetic unit of magnetic moment (e.m.u) in C.G.S system. Both the spin and rotation of electrons around the nucleus are responsible for magnetic dipole moment in the atom. These tiny magnetic dipole

moments of electrons respond to external magnetic fields and give rise to magnetization 'M', which can be defined by the net magnetic moment 'μ_{total}' in unit volume of the material.

$$M = \frac{\mu_{total}}{V} \qquad (1.1)$$

The electrons spin in atomic structure originates magnetization. The total magnetic field 'B' depends on magnetization and externally applied field, i.e.

$$B = B_{ext} + \mu_0 M \qquad (1.2)$$

Where 'B_{ext}' represents the strength of external magnetic field and 'μ_o' is permeability of free space, which is, 4π x 10^{-7} NA^{-2}. The magnetic field strength 'H' depends only on strength of the external magnetic field, that is,

$$H = \frac{B_{ext}}{\mu_0} \qquad (1.3)$$

Inserting value of eq. (1.3) in eq. (1.2), resulting,

$$B = \mu_0 (M + H) \qquad (1.4)$$

The magnetization 'M' and external field 'H' can be related by the relation;

$$M \propto H$$

$$M = \chi H \qquad (1.5)$$

Where 'χ' is the proportionality constant called magnetic susceptibility, and it is the ratio of magnetization and the magnetic field.

1.3.1 Classification of Magnetic Materials

Magnetic properties of any material arise due to the interactions of unpaired electrons and are mostly found in transition metals and their compounds due to the unpaired 'd' and 'f' electrons of the metal. Paramagnetism, diamagnetism, ferromagnetism, antiferromagnetism and

ferrimagnetism are general types of magnetic behaviors which can, typically, be analyzed by their magnetic susceptibility (χ).

Paramagnetism is class of magnetism in which individual magnetic moments are randomly arranged. Paramagnetic materials are highly affected by external applied field because this field tends to align the dipoles. These materials have zero net magnetic moment as shown in Figure 1.1(a). The induced field is proportional to the applied field at high temperature and at small values of field; the magnetization has same direction as applied magnetic field. Paramagnetism varies inversely with temperature, i.e.

$$\chi = \frac{C}{T} \qquad (1.6)$$

Various paramagnetic materials behave as ferromagnetic below Curie temperature T_c.

Diamagnetic is that form of magnetic material in which every atom has net zero magnetic dipole moment in the absence of applied magnetic field as shown in Figure 1.1(b). Any conductor shows diamagnetic behavior in the presence of externally applied field because the tiny current loops of the material tend to align themselves in opposite direction to the applied magnetic field. In superconductor, when there is no resistance for formation of current loops then it behaves as perfect diamagnetic materials.

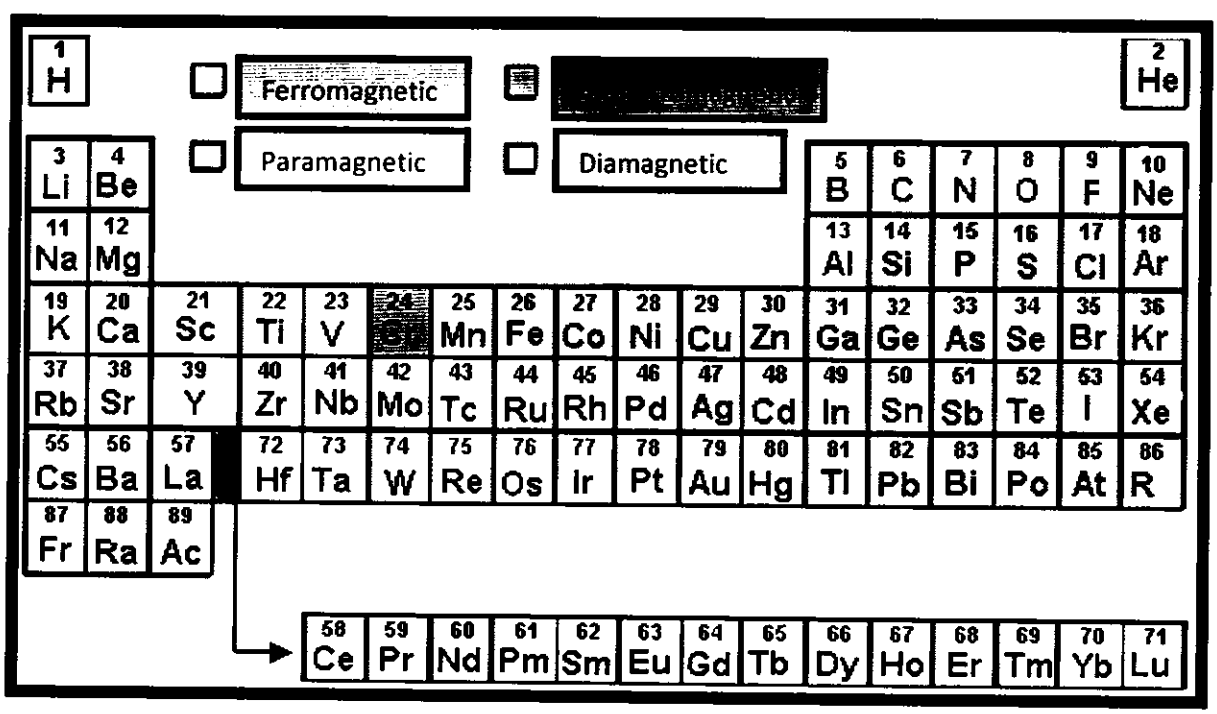

Figure 1.1: Identification of classifications of magnetic materials from periodic table.

Ferromagnetic are those materials in which all the individual magnetic moments having same magnitude are aligned in same direction even in absence of externally applied magnetic field as shown in Figure 1.1(c). At atomic level, these materials have long range of ordering which causes the unpaired electron spins to lineup parallel with each other a specific region, known as called domain. Ferromagnets reveal parallel alignment of magnetic moments within a domain resulting high net magnetization even in the absence of applied field. Ferromagnetic materials have ability to stay magnetized to some extent after being subjected to externally applied magnetic field. This ability to stay magnetize is called hysteresis. On removal of applied field, the part of saturation magnetization which is preserved is termed as remanence. Due to thermal disturbance, ferromagnetic materials lose their ferromagnetic property at a maximum temperature, called T_c. i.e;

$$\chi = \frac{C}{T - \theta} \qquad (1.7)$$

Each atom of ferromagnetic materials has strong magnetic dipole moments in the absence of applied filed due to uncompensated electron spins. These materials are strongly attracted to either pole of a magnet. Spontaneous magnetization and magnetic ordering temperature are two different characters of ferromagnetic materials. Some important concepts for ferromagnetic materials are the magnetostatic energy, magneto-crystalline anisotropy, magnetostrictive energy and domain wall energy.

Antiferromagnetic materials have zero net magnetic moment having opposite magnetic moments of same magnitude as shown in Figure 1.1(d). In antiferromagnetic materials, both A sublattice and B sublattice moments are opposite in direction but exactly equal in magnitude gives net zero moment. The behavior of susceptibility above critical temperature, Neel temperature (T_N), directs towards antiferromagnetism. Beyond T_N, the antiferromagnetism is lost and the system moves towards paramagnetism.

Ferrimagnetic is that form of magnetic material in which two magnetic moments of different strength are arranged in antiparallel fashion, which enables the material to have net magnetic moment as shown in Figure 1.1(e). In ferrimagnetic materials, the sublattice moments of A and B are not equal in magnitude which results in a net magnetic moment within a domain.

Hence, ferromagnets and ferrimagnets have very different magnetic ordering. Beyond T_c, the ferrimagnets become disordered and lose their magnetization. The nature of magnetic moments in ferromagnetic, antiferromagnetic and ferrimagnetic materials decreases with increasing temperature.

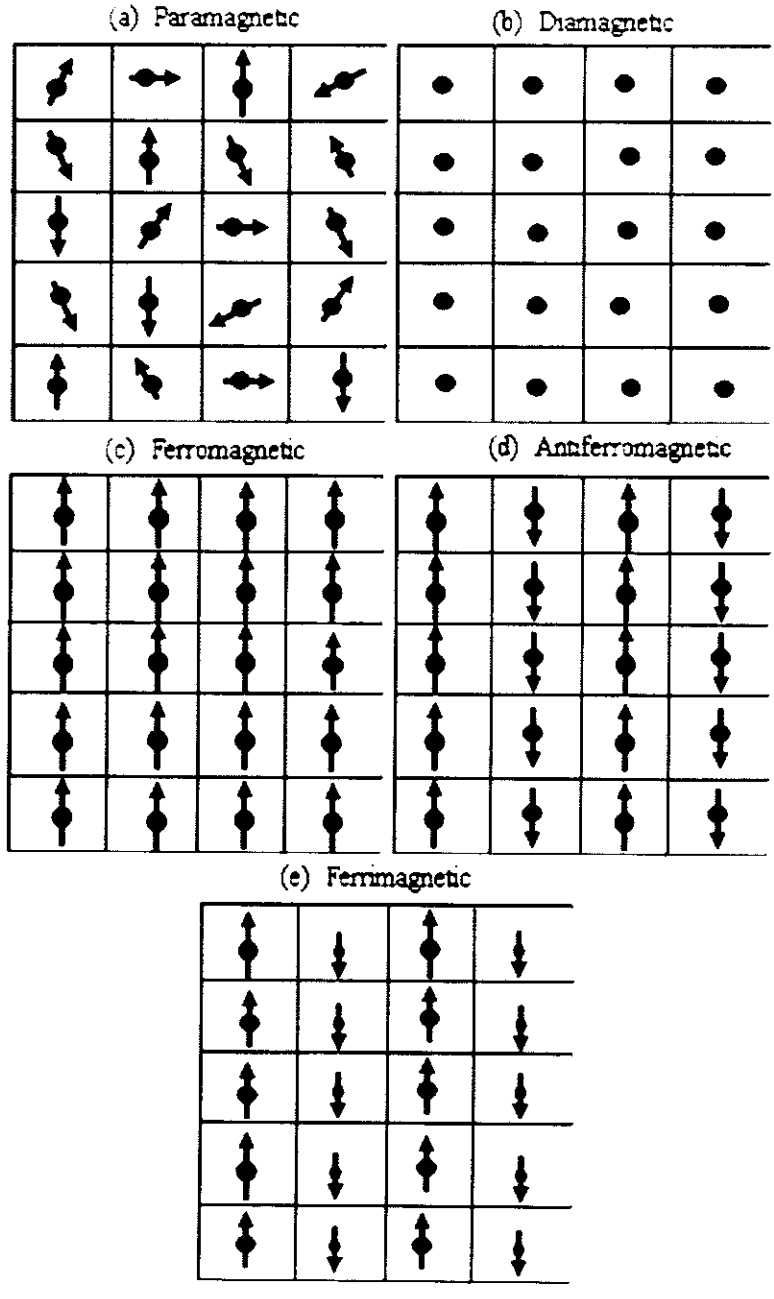

Figure 1.2: Classification of magnetic materials, a) Paramagnetic, b) Diamagnetic, c) Ferromagnetic, d) Antiferromagnetic, and e) Ferrimagnetic.

1.4 Domains

The ferromagnetic materials in demagnetized state have a large number of small regions which are known as domains. In 1907, Weiss proposed that the ferrimagnets or ferromagnets composed of domains having fixed orientation of magnetic moments as shown schematically in Figure 1.3. Domain boundaries or domain walls are the only way to separate domains of an atom. The formation of domains allows the material to minimize its total magnetic energy. Weiss explained that magnetic materials have large amount of domains that are saturated in a different direction. Keeping in mind the concept of domains, the ferromagnetic materials can easily be demagnetized even below T_c.

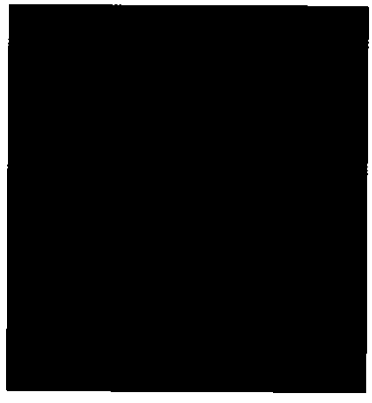

Figure 1.3: Illustration of domains in ferromagnetic materials [4].

In 1907, Weiss proposed that magnetic domains inside the material have net zero magnetization when the domains are magnetized in different directions. These domains try to minimize demagnetization fields and in some cases eliminate completely. Domain walls separate one domain from another [4]. A domain wall includes Bloch wall, Neel wall and Cross-Tie wall. Figure 1.4 is comparison of Bloch wall, with charged surface on the external surface of the sample and Neel wall, with charged surface internal to the sample.

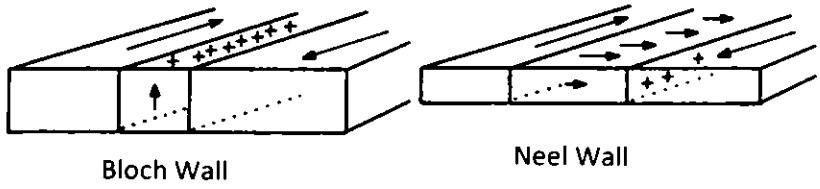

Figure 1.4: Representation of Bloch wall and Neel wall [5].

Once domains form, the orientation of magnetization in each domain and the domain size can be determined by magnetostatic energy (MS), crystal anisotropy, magnetostrictive energy and domain wall energy [5, 6]:

1.4.1 Magnetostatic or Demagnetization Energy

The magnetic field around a magnetized material acts to magnetize the material in the opposite direction from its own magnetization. This causes MS which is dependent on the shape of material. By the reduction of net external field, the MS can be reduced through the formation of domains inside the material.

In ferromagnetic materials, MS depends on the alignment of moments at finite temperatures, as thermal vibrations causes misalignment of magnetic moments which reduces MS of the material. At 0K, all the magnetic moments are aligned parallel in ferrimagnetic materials. Hence, MS depends on the temperature and relative alignment of magnetic moments of the material. Domain formation in a saturated magnetic material is driven by the MS of the single domain state (Figure 1.5 (a)). Introduction of 180° domain walls reduces the MS energy but raises the wall energy (Figure 1.5 (b)); 90° closure domains eliminate MS energy but increase anisotropy energy in uniaxial material (Figure 1.5 (c)).

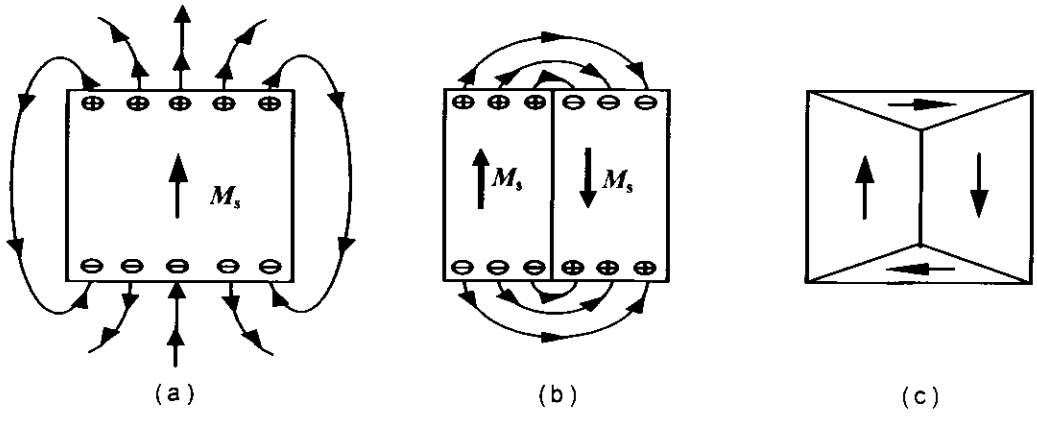

Figure 1.5: a) Single domain having large stray field, **b)** Reduction in two domains or reduction of MS, and **c)** Division of sample in four domains (making MS zero) [6].

1.4.2 Magneto-Crystalline Anisotropy Energy

In material science, there are some materials in which domain magnetization tends to align crystal along easy axis. When field is along the easy axis then magnetic behaviors such as magnetization, saturation or demagnetization of these materials can easily be varied. The difference in energy used for alignments of domains in easy or hard direction is known as magneto-crystalline anisotropy energy. The energy required to rotate the magnetic moment for easy axis to hard axis is called anisotropy energy.

The materials such as ferrites, this magneto-crystalline anisotropic energy can be expressed as:

$$E_K = K_1 \sin^2\theta + K_2 \sin^4\theta \ldots \text{(hexagonal)} \qquad (1.8\,(a))$$

$$E_K = K_1(\alpha_1^2\alpha_2^2 + \alpha_2^2\alpha_3^2 + \alpha_3^2\alpha_1^2) + K_2(\alpha_1^2\alpha_2^2\alpha_3^2 + \cdots)\ \text{(cubic)} \qquad (1.8\,(b))$$

Where 'K' is anisotropic constant, 'θ' is angle between direction magnetization and easy axis and 'α' is direction cosines (equation 1.8 (a and b)). When the magnetization points are along hard direction then the crystal has higher anisotropy energy and vice versa. By the formation of domains, the magnetization is pointed along the easy axis, which results in decreasing net anisotropy energy.

1.4.3 Magnetostrictive Energy

When magnetic field is applied on the material, there may change in its dimensions resulting as a change in magnetostrictive energy. The magnetostrictive energy can be lowered by a reduction in the size of the domains, requiring the formation of more domains. The strain and effective strain (caused by applied stress) are the change in lengths or simply strain [7] which can be expressed as;

$$\lambda = \frac{\Delta L}{L} \qquad (1.9)$$

where 'λ' represents magnetically induced strain. At magnetic saturation, the value of 'λ' is termed as saturation magnetization 'λ_s', which depends on amount of magnetization and applied magnetic field.

1.4.4 Domain Wall Energy

The variation (increase/decrease) in the width of domain walls due to the growth or shrinkage of domains forms domain wall energy.

The rotation of the magnetic dipoles (toward applied field) and change in the domain volume results the changes in domain magnetization (Figure 1.5). In the first case, for the rotation of the magnetization in a crystal from one axis to another, a certain amount of anisotropy energy is needed. In the second mechanism, the volume of the domain changes while the magnetization direction is unchanged. This changing is in its contribution to the bulk magnetization. The direction of magnetization to applied field is responsible for the change in magnetization intensity of domains. The intensity depends on magnetization in such a way that if the magnetization direction is close to applied magnetic field then the magnetization intensity in the domain increases and decreases when magnetization direction is far to applied magnetic field. The domain volume changes due to motion of the domain wall. This movement is originated by a torque that rotates the moments of the domain in line with the field, moving the center of the wall toward the domain opposed to the field. Consequently, the volume of the domains whose direction is favorable is increased whereas, the volume of domains decreases with unfavorable direction [5].

1.5 Magnetization Curve and Hysteresis Loop

In ferromagnetic materials, when external applied field is increased then atomic dipoles of the material align themselves along applied magnetic field which results in increase in magnetization of material and when the applied field is removed then magnetization does not follow increasing magnetization curve due to the internal fraction. The irreversibility is termed as hysteresis. Magnetization 'M' is a function of strength as well as direction of the magnetizing field 'H'. Magnetic flux density and field strength varies non-linearly in ferromagnetic materials such that the magnetic field strength increases up to a point where further increase in field will result in no further change in flux density. This condition is known as magnetic saturation (M_s) and it is defined as the maximum amount of field that a material can acquire as shown in Figure 6. M_s depends on how strongly/densely; the dipole moments on the atoms of the materials are packed together.

The atomic dipole moments depend on the nature, configuration and electronic structure of atom, while the packing density is determined by crystal structure and occurrence of non-magnetic elements contained in structure. When the field is reduced linearly then the curve follow different path towards zero field strength, the amount by which it will offset from original curve is termed as remanence. When externally applied magnetic field is removed then left behind magnetization is termed as remanence and is denoted by M_r. It is taken on the intersection point of loop with vertical magnetization axis in hysteresis curve as shown in Figure 1.6. When it is plotted for all values of magnetic field strength it gives an S-shape loop. Loop thickness describes the coercivity of the material (H_c), defined as the intensity of applied field required to decrease the magnetization to zero; subsequent to magnetization of the material attains saturation. The coercive field or H_c is measured in Area/meter (A/m) or Oersted (Oe). The value of H_c for hard or permanent magnet is large and vice versa. Its practical effects might because of a slow release due to remaining magnetic field continuing to attract the armature when applied current is removed. M_r is low in soft magnets and is high for permanent magnets. Hence, the type of magnet is determined by the value of the remnant induction [8].

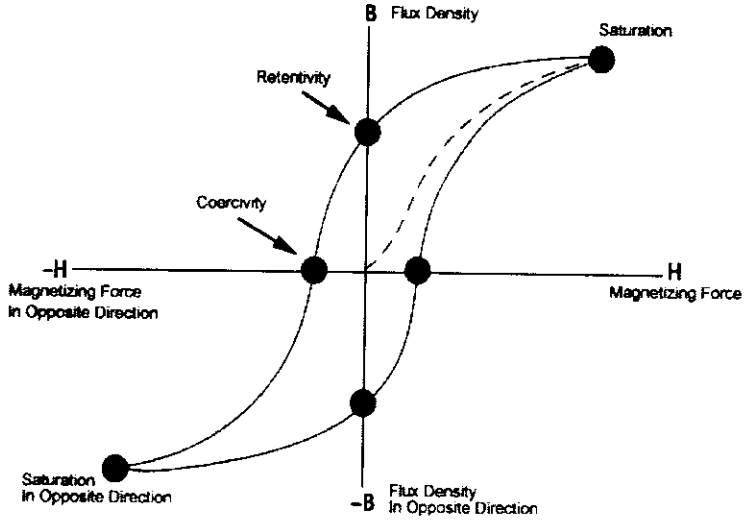

Figure 1.6: Hysteresis loop of magnetic material [9].

The low coercive field for soft ferrites, *i.e.* $H_c < 80$ A/m, determines their application in dynamic fields. These ferrites have various applications in high frequency inductors, switching cores, microwaves (from magnetic elements) and transformers [8].

1.6 Temperature Effect on Magnetism

As the temperature increases, the thermal oscillation competes with the tendency for the magnetic dipoles to position themselves in a specific way. When the temperature rises beyond a certain point, the material can no longer maintain its intrinsic domain formation and becomes paramagnetic. 'T_c' and 'T_N' are used to mark these transitions.

1.6.1 Curie Temperature

The individual carriers of magnetic moment do not interact with one another normally. In ferromagnetism, exchange forces are very large but at certain temperature the thermal energy dominates exchange forces which produces random effects. This definite temperature is known as Curie temperature (T_c). It is the point above which all ferromagnetisms lose their ferromagnetic characteristic. In ferromagnetic materials, the moments are partially aligned within domains below T_c. When temperature is raised from below Curie point, then thermal fluctuations gradually destroy these alignments continuously until net magnetization turns to zero. Furthermore, above T_c the materials behave as paramagnetic material. At T_c, saturation magnetization goes to zero and its effects are reversible.

1.6.2 Neel Temperature

The temperature at which thermal energy is sufficient to annihilate magnetic ordering inside the material is called Neel temperature (T_N). At T_N, the antiferromagnetic materials become paramagnetic materials.

1.7 Superparamagnetism

A magnetic material with single domain magnetic moments having no hysteresis loop is termed as superparamagnetic material. Materials with zero coercivity shows M-H curves of superparamagnets resemble to ferromagnets at saturation by following Langevin behavior. In ferromagnets, the surface energy gives space to the domains to spontaneously switch their polarization directions, when their size reduces below a certain value. The magnetization behavior of superparamagnetic particles at all fields is same apart from large value of fields. Superparamagnetism includes two main requirements; firstly, superparamagnetism confirm no

hysteresis in magnetization curve. Secondly, for isotropic curve, the magnetization must depend on the temperature to an amount that at different temperatures all curves should superimpose.

Superparamagnetic demagnetization occurs without H_c because it is not the result of the action of an applied field but rather of thermal energy. Lack of hysteresis and universal curve of M vs. H / T are the two main qualities of superparamagnetic materials. The hysteresis parameter like the coercive field gives insight about demagnetization of field that provides important indication for many applications. For many other delicate applications like sensors and medical imaging, very fine grained magnetic particles are needed.

The heat treatment by temperature or time, or both increases the magnetic property of Iron ions participating into a magnetite phase shows different magnetic behaviors. The magnetic behaviors depend on the particle size, the heat-treatment schedule and on the temperature [10, 58]. Due to a fast relaxation of the magnetization, these nanoparticles of magnetite behave as superparamagnetic below the magnetic transition temperature [11]. These alignments or re-alignments are constantly occurring inside the material depending on the temperature and the particle volume. However, it is important to detect the magnetite showing super-paramagnetism with very fast relaxation for their interesting behavior.

1.7.1 Relaxation Time

When applied field changes then magnetization of a colloidal ferrofluids relaxes by particle rotation in the liquid and the rearrangement of the magnetic dipole vector within the particles. In this case, the magnetic dipole is locked as the particle undergoes rigid body rotation. In the second mechanism, the relaxation is due to dipole jump from one easy axis to another.

The particle rotation occurs due to rotational Brownian motion, and is expressed as,

$$\tau_B = \frac{3V_{h0}}{kT} \qquad (1.10)$$

Where V_h is the particle hydrodynamic volume, η_o the viscosity of the carrier liquid and τ_B is Brownian rotational diffusion time.

In the absence of a field, the magnetization of a single domain uniaxial ferromagnetic particle can have two possible orientations. The magnetization fluctuations of particles are induced by characteristic time at high values of thermal energy ($KV << k_\beta T$), i.e.

$$\tau_N = \tau_0 e^{[\frac{KV}{k_\beta T}]} \qquad (1.11)$$

Where τ_0 is a characteristic time, typically having the approximate value 10^{-9} s.

The relaxation mechanism can bitterly decide intrinsic or extrinsic superparamagnetism. When relaxation occurs by the Neel mechanism ($\tau_N << \tau_B$) then suspension possesses intrinsic superparamagnetism and when the relaxation is dominated by the Brownian mechanism ($\tau_B << \tau_N$), the suspension exhibits extrinsic superparamagnetism. The materials that got less time of experiment then the relaxation time form ferromagnetic materials [12]. Because τ_N has an exponential dependence on V, it is sharply dependent on particle size [13], therefore, for the same magnetic material the dominant mechanism will depend on the particle size.

1.8 Ferrites

Ferrites are complex oxides (ceramics) containing Iron. Ferrites exhibit interesting magnetic, optical and physical properties. Mechanically, ferrites are rigid and when handled roughly they lose their rigidity. Electrically ferrites are insulators [14]. At room temperature, the resistivity of ferrites varies from 10^{-2} Ω-cm to 10^{11} Ω-cm, depending on their chemical composition [15]. Their coloration is from grey to black. Iron oxide is well known class of spinel ferrites due to its natural occurrence, spontaneous magnetization, high magnetic permeability and low conduction losses [16]. From magnetic point of view, ferrites are mostly ferrimagnetic materials. Magnetic properties of Zinc ferrites are significantly affected by particle size. Recently, many functionalized magnetic nanoparticles having multi-functional properties are used in sensors and medical [17].

1.9 Types of Ferrites

In view of Crystal structure, ferrites are classified into three main different types;

- Spinel Ferrites
- Hexagonal Ferrites
- Ortho Ferrites

1.9.1 Spinel Ferrites

The superexchange interaction of cations and Oxygen anions at different interstitial sites form spinel ferrites. The difference in magnitude of magnetic moments and number of magnetic ions at interstitial sites are responsible for various changes in properties. The spinel structure has two interstitial sites; (i) Tetrahedral Site (A-Site) and (ii) Octahedral Site (B-Site) with face centered cube (FCC) lattice site (Oxygen atom). The general formula for cubic spinel structure is $MO{\cdot}Fe_2O_3$ where M can be Ba, Sr and Pb.

1.9.2 Hexagonal Ferrites

In hexagonal ferrites, the cations have five folds symmetry. The magnetism in hexagonal ferrites is due to exchange mechanism. The moments of A and B sites have antiparallel alignment of spins; therefore, the net magnetization is less strong as compared to metallic ferromagnetic materials.

To understand the structure of this complex unit cell, one needs to know the relationship between hexagonal and cubic structure. Both are arranged in a particular sequence in the form of layers as shown in Figure 1.7. The structure is hexagonal closed packed when these layers are mound in *ABABAB*...sequence with its third layer directly over first. When layers are arranged in *ABCABC*.... sequence then the result will be FCC structure as sequence does not replicate itself until forth layer. Figure 1.7 shows a unit cell which consists of 10 layers of large Ba^{2+} and O^{2-} ions. Eight layers consist of Oxygen and two of Barium. These ten layers contain four blocks, i.e.; two cubic and two of them are hexagonal. In case of cubic block, Oxygen ions arrangement is just like the spinel cubic structure [9].

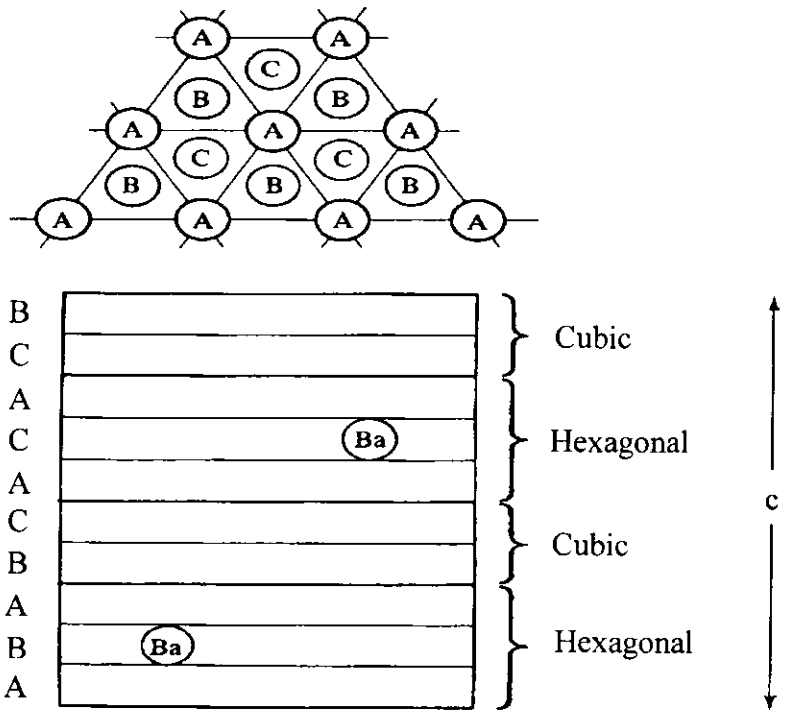

Figure 1.7: Illustration of Barium ferrite structure [9].

1.9.3 Ortho Ferrites

Ortho ferrite is a type of ferrites that has ortho-rhombic crystal structure and belongs to Pb_{nm} space group. The general formula for ortho-ferrites is R. FeO_3; where 'R' represents rare earth elements. Most of the ortho ferrites are weakly ferromagnetic. Lanthanum Orthoferrite ($LaFeO_3$) and Dysprosium Orthoferrite ($DyFeO_3$) are common examples of Orthoferrite [18].

As current research work is on spinel ferrites; hence, only spinel ferrites are to be discussed in details.

1.10 Spinel Ferrite Structure

The cubic spinel structure has the molecular/general formula AB_2O_4, where A is a divalent metal ion (e.g. Mg^{2+}, Zn^{2+}, Fe^{2+}, etc.) and B denotes a trivalent ion (Al^{3+}, Fe^{3+}, etc.) having crystallized in Fd-3m space group. The spinel structure of ferrites possessed by mineral spinel ($MgAl_2O_4$) was determined by Bragg and Nishikawa in 1915 [19]. The particular preference of ions for octahedral or tetrahedral coordination decreases in the following order [8]:

$$Cr^{3+} > Mn^{3+} > Ni^{2+} > Co^{2+} > Mg^{2+} > Ti^{3+} > Fe^{2+} > Fe^{3+} > Mn^{2+} > Zn^{2+}.$$

The proximity of the Fe^{2+} and Fe^{3+} ions indicates that they can easily interchange their positions between the A and B sites.

Some sort of structural disorders have been detected in spinel structures. The shift of Oxygen and the metal cations in the B sites of spinel structure can create local permanent dipoles in ferrites, which could interact spontaneously in the anti-parallel orientation. Cobalt ferrites have the properties of inverse spinel ferrite structure. All the cubic spinel ferrites are magnetically soft except Cobalt ferrites which are magnetically hard. The Cobalt ferrites due to moderate saturation magnetization (80 $emug^{-1}$) and large magnetic anisotropy ($2.65\text{-}5.1 \times 10^{6} erg/cm^{3}$) have attracted a lot of attention [20].

The spinel structure has two interstitial sites; (i) Tetrahedral site (A) and (ii) Octahedral site (B). In a unit cell, there are total 56 ions which include 8, 16 and 32, M^{2+}, Fe^{3+} and O_2^- ions, respectively.

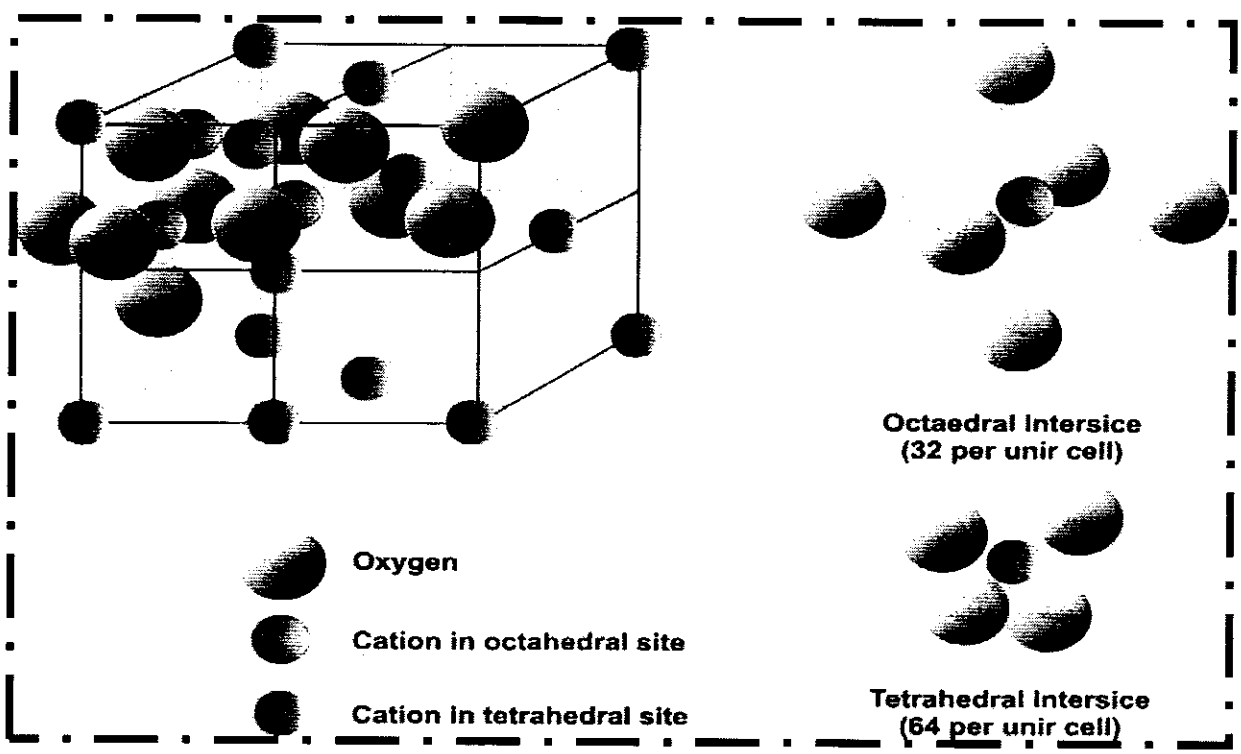

Figure 1.8: Cubic spinel structure [1].

1.10.1 Tetrahedral Sites

Spinel structure has 64 tetrahedral A sites and the cations occupy $\frac{1}{8}$ of the tetrahedral site; such as,

64 Tetrahedral A site / 8 = 8

In tetrahedral site, four Oxygen atoms are at lattice positions, while the interstitial atom is in the center of tetrahedral. Out of four atoms, only the fourth atom sits in the symmetrical position on top and the remaining three are in the plane touching each other.

1.10.2 Octahedral Sites

Spinel structure has 32 octahedral B sites and the cations occupy $\frac{1}{2}$ of the octahedral site; such as,

32 Octahedral B site / 2 = 16

In octahedral site, four regular atoms are positioned in a plane; the other two are in asymmetrical position just above or below as shown in Figure 1.8. In FCC, there are 4 octahedral sites per unit cell as shown in Figure1.9.

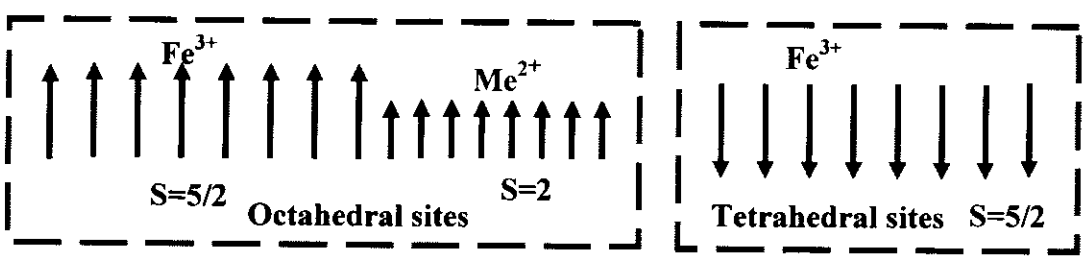

Figure 1.9: Tetrahedral and Octahedral Sites in FCC lattice.

1.11 Types of Spinel Ferrites

According to distribution of cations on tetrahedral (A) site and octahedral (B) site, the spinel ferrites are categorized into three types.

- Normal Spinel Structure
- Inverse Spinel Structure
- Mixed Spinel Structure

1.11.1 Normal Spinel Structure

In normal spinel structure, non-magnetic ions are occupying A site and consequently there is no AB interaction. The negative BB interaction now makes itself felt and the trivalent Irons ions align themselves in an anti-parallel fashion, producing zero net magnetization [21]. The general formula for normal spinel structure is $MO.Fe_2O_3$. In normal spinel structures, 8 tetrahedral sites are occupied by the eight M^{2+} and 16 octahedral sites occupy Fe^{3+} ions [22]. i.e;

Normal Spinel: 8 M^{2+} in A-Site, 16 Fe^{3+} in B-Site.

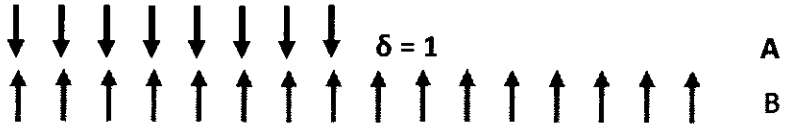

Figure 1.10: Normal spinel strucutre.

The typical example of normal spinels is $ZnO.Fe_2O_3 = ZnFe_2O_4$.

1.11.2 Inverse Spinel Structure

In inverse structures, the AB interactions lead to a parallel arrangement within each sublattice. As the divalent ions have no magnetic moment, the net magnetization vanished [21]. In inverse structures, B sites are occupied by the nonmagnetic ions, whereas the Iron is evenly divided between the two lattice sites. The general molecular formula of inverse spinel structure is $(MFe_2).O_4$. In inverse spinel structure, one half of B site ions are placed in tetrahedral sites, while other half and whole of A site ions are located in the octahedral sites. There are $8M^{2+}$ ions which contain 8 octahedral sites and remaining 16 Fe^{3+} ions are divided into two sites; the 8 inhabited octahedral sites and 8 tetrahedral sites as shown in Table 1 [22]. i.e;

Inverse Spinel: 8 Fe^{3+} in A, 8 M^{2+} + 8 Fe^{3+} in B.

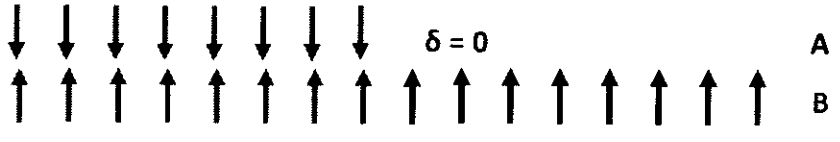

Figure 1.11: Inverse spinel structure.

Mostly, ferrites have inverse spinel structure. The common example of inverse spinel ferrite is $CoO.Fe_2O_3 = Fe\ CoFeO_4$ [8].

Table 1: Metal ion arrangements in spinel ferrite unit cell with composition $MO.Fe_2O_3$.

Types of Interstitial Site	Number Available	Number Occupied	Normal Spinel	Inverse Spinel
Octahedral	64	8	$8M^{2+}$	$8Fe^{3+}$
Tetrahedral	32	16	$16\ Fe^{3+}$	$8Fe^{3+} + 8M^{2+}$

1.11.3 Mixed Spinel Structure

In mixed spinel structures, the trivalent Iron is un-symmetrically distributed between the two types of sites and if the AB interaction is dominant, there will be a net magnetization [22]. The general formula of mixed spinel ferrites is $(A_{1-x}B_x)\ (A_xB_{2-y})\ O_4$. Mixed spinels ferrites show interesting magnetic properties for numerous applications besides only one type of trivalent metal ion or divalent metal ion. Also these ferrites have variation in their composition. i.e;

Intermediate structure: Not perfectly normal or inverse structure.

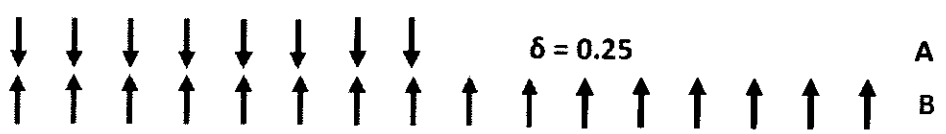

Figure 1.12: Mixed spinel structure.

The common examples of mixed ferrites are Magnesium-Zinc and Manganese-Nickel ferrites [8].

1.12 Magnetic Classification of Ferrites

Magnetic materials are classified into two main types on the basis of their ability to be magnetized and demagnetized. Soft ferrites are easily magnetized or demagnetized whereas hard ferrites are difficult to magnetize or demagnetize [7].

- Soft Ferrites
- Hard Ferrites

1.12.1 Soft Ferrites

The magnetic materials that can be easily magnetized or demagnetized are known as soft ferrites. This indicates that soft ferrites have low coercive field and high magnetization, which is very useful in many applications. Soft magnetic materials have very thin and long hysteresis loop. Due to this, the energy loss in soft ferrites is quite low. Nickel, Cobalt, Manganese and Iron are common examples of soft ferrites which are very useful in various applications such as transformer cores, inductors, recording heads, magnetic tapes, disks and microwave devices [6]. The amorphous soft magnetic alloys are very strong and have enormous corrosion resistance due to absence of long range ordering. High resistivity, high permeability, low eddy current losses and stable at wide range of temperatures are diverse advantages of soft ferrites. These advantages made soft ferrites dominant over all other magnetic materials [23].

1.12.2 Hard Ferrites

The magnetic materials that are difficult to magnetize or demagnetize are termed as hard ferrites. Hard ferrites are also treated as permanent magnets due to very high coercivity and wide hysteresis loop. Alnico and rare Earth metal alloys are typical examples of hard magnetic materials [24]. Hard ferrites are ferrimagnetic having low remanence and high coercive field. Their applications are normally into moderate demagnetizing fields and permanent magnet motors. These are formed by the combination of Iron, Barium or Strontium oxides [25].

1.13 Crystalline Structure of CoZn Ferrite Nanoparticles

Cobalt Zinc ferrite nanoparticles have crystalline spinel structure. The general formula for spinel structure is $A^{2+}B_2^{3+}O_4^{2-}$. This formula points crystallite in cubic crystalline system. In spinel structures, cations A and B occupy tetrahedral or octahedral sites and oxide anions arranged in cubic closed packed lattice. These sites (A, B) could have divalent, trivalent and quadrivalent cations in spinel structure and the anions are normally oxide. Under different charges, A and B sites could have same metal. Fe_3O_4 or $Fe^{2+}Fe^{3+}O_4^{2-}$ are common example of it.

1.14 Ferrofluides

Ferrofluides are colloidal liquids that composite of ferrimagnetic or ferromagnetic nanoparticles, suspended in organic solvent (water) and layered with a surfactant to retain clumping. Surfactant having long chain hydrocarbons consists of polar head called hydrophobic part and a more extended hydrocarbon tail called hydrophilic part [26]. In ferrofluides, generally Kerosene, Hexadecane and Oleic acid are used as surfactant. Ferrofluids are stable against gravitational and field gradient. The stickiness to magnets taking on three dimensional shapes when magnetic field is applied and density changes in proportion to applied magnetic field strength are some valuable properties of ferrofluids. In the absence of externally applied field, the magnetic moments of particles are randomly distributed, hence, the ferrofluides does not preserve magnetization due to net zero magnetization of field, that's why; ferrofluides are often termed as superparamagnetic besides ferromagnetic materials [27]. When magnetic field is applied on ferrofluids then moments of particles immediately align themselves along the magnetic field. Ferrofluides appear as homogenous magnetic liquid in field gradient that moves to highest flux region. This shows that ferrofluides can specifically controlled by an externally applied magnetic field and value of magnetization of fluid. Hence, the retention force of ferrofluides could be used via magnetic field in region or by varying magnetization.

1.15 Application of CoZn Ferrite Nanoparticles

High value of electrical resistivity of ferrites indicates that these are very significant magnetic materials and can have extensive applications in modern technologies, especially at high frequencies. Ferrites are used widely due to their following properties;

- Ferrites are part of high flux and low power transformers, which are used in television
- Small antennas are made by winding a coil on ferrite rod used in transistor radio receiver
- Ferrites are used in high frequency transformer core and computer memories such as computer hard disk, floppy disks, credit cards, audio cassettes, video cassettes and recorder heads

- Ferrites used in magnetic tapes and disks are made of very small needle like particles of Fe_2O_3 or CrO_2, which are coated on polymeric disk. Each particle is a single domain of size 10-100 nm
- Ferrites are used to produce low frequency ultrasonic waves by magnetostriction
- The manufacturing of many inductor cores along with capacitors circuits in telephone system were done with soft ferrites, but now a days, these are replaced by solid state devices. Cobalt-Zinc and Nickel-Zinc soft ferrites are mostly used in core manufacturing
- Many ferrites have applications in circulators, switch phase shifters, isolators, radar circuits and many other microwave devices
- Ferrites are used as electromagnetic wave absorbers at low dielectric values
- Ferrites are functional in drug delivery and hyperthermia of cancer treatment
- Ferrofluids are used in cooling materials as speakers. They cool the coils with vibrations

1.16 Literature Survey of CoZn Ferrite Nanoparticles

Nanocrystalline ferrites are currently highly entertained because of their exceptional purposeful properties and applications in industrial, medical, electronics and various research areas (nanostructures). Cobalt ferrite is significant due to high intrinsic properties such as high value anisotropy, saturation magnetization, coercivity, mechanical hardness and chemical stability [28, 29]. Islam et al. [30] reported decrease in magnetization saturation by increasing contents of Zinc in Cobalt nanoparticles. Laser irradiation effects on cation allocation of $Co_{0.6}Zn_{0.4}Fe_2O_4$ nanoparticles were investigated by Tawfik et al. [31] and found changes in IR absorption bands by replacement of $Fe^{3+}O^{2-}$ bond lengths from F^{3+} ions. Ghose and Dey [32] fabricated $Co_{0.2}Zn_{0.8}Fe_2O_4$ nanoparticles via coprecipitation route and established magnetization decreases by increasing values of particle size. Arulmurugan et al. [33] reported substitution of Cobalt with Zinc shows betterment in magnetic properties of nano-crystalline ferrites. They found that saturation magnetization decreases with the increase of Zinc contents in prepared nano ferrites. Ana Maria Rangel et al. [34] synthesized nanoparticles via powdered coprecipitation route and evaluated that on heating precipitates triple hydroxide to 400 °C for 5 hours; they show well crystallite size. Moreover, particles are processed at short calcinations time and low temperature. They also evaluated that occurrence of sharp XRD peaks and low coercivity at 1350°C - 1400°C

sintering temperature confirms synthesized ferrite nanoparticles were soft ferrites. D. S. Mathew et al. [35] found that Cobalt ferrites have inverse spinel structures with Cobalt ions at octahedral site and Iron ions are distributed in both octahedral and tetrahedral sites while Zinc ferrites have normal spinel structure with Iron at octahedral site and Zinc ions at tetrahedral sites. Recently, spinel ferrites have extensively studied due to their exceptional electrical and magnetic properties [36]. Chiu WS et al. [37] found distorted cubic spinel structures and variation in magnetic properties when Zinc substituted Cobalt ferrite nanoparticles were fabricated. Microwave induced combustion technique was used by Y. Koseog˘lu a et al. [38] for preparation of Cobalt doped Zinc ferrites and found that ferrites were spinel structured with crystalline size of 35nm-39nm. It is observed that blocking temperature of synthesized particles increases with increase in Co contents that reflects magnetic phase transitions of magnetic nanoparticles. Waje et al. [39] synthesized $Co_{0.5}Zn_{0.5}Fe_2O_4$ nano-ferrite through sintering and mechanical alloying and observed that for measured frequency range permittivity is constant, however, it varies with variation in sintering temperature. Generally, permeability varies with frequency as well as sintering temperature of nanomaterials. M. H. Yousefi et al. [40] prepared Cobalt Zinc nanopowders via combustion method and found out mean crystalline size ranges 37nm and reduction in strain factor on annealing. Moreover, T_c shows remarkable reduction at nanosized due to reduction in superexchange interactions. Sonal Singhal et al. [41] used sol-gel scheme for preparation of Zinc substitute Cobalt ferrite nanoparticles and observed that with variation of concentration and increasing value of annealing temperature the growth size, x-ray density and lattice parameter increases. Saturation magnetization of synthesized nanoparticles initially increases from $CoFe_2O_4$ to $Co_{0.6}Zn_{0.4}Fe_2O_4$ and then decreases till $ZnFe_2O_4$. $Co_{0.5}Zn_{0.5}Fe_2O_4$ nanoparticles was reported by M. Mozaffari et al. [42] synthesized via chemical coprecipitation method at room temperature. They estimated crystalline size of nanoparticles within 6nm - 8nm and show less magnetization saturation of nanocrystallite $Co_{0.5}Zn_{0.5}Fe_2O_4$ as compared to bulk because of surface effects and spin canting. Electrospinning and heat treatment was used to fabricate $Co_{1-x}Zn_xFe_2O_4$ ($0 \leq x \leq 0.5$) nanofibres ferrites by X.Q. Shen et al. [43]. They investigated crystallite size and diameter of nanofibres within range of 50 nm and 110 nm – 130 nm, respectively. The saturation magnetization of synthesized $Co_{1-x}Zn_xFe_2O_4$ nanofibres initially increases up to $x = 0.3$ and then decreases with increasing value of Zinc contents. Significant

applications of nanofibres are in flexile magnets, nanoelectronics, microwave absorption devices and magnetic sensors. A. R. Jelvani et al. [44] prepared $Co_{0.5}Zn_{0.5}Fe_2O_4$ nanopowders through three dissimilar synthesis techniques and concluded H_c, T_c, M_r and M_s depends on method to be prepared as well as nanocrystalline size. Zinc substituted Cobalt $Co_{0.8}Zn_{0.2}Fe_2O_4$ ferrite nanoparticles were synthesized by Harshida Parmar et al. [45] by using modified microwave combustion route and then post treatment of nanoparticles was taken through washing of 0.1M HCl and NaCl; which results in fine quality ferrite nanoparticles for magnetic and neutron studies. J. Lo`pez et al. [46] synthesized $Co_{1-x}Zn_xFe_2O_4$ nanoparticles via chemical co-precipitation technique and explored that particle size decreases with increasing percentage concentration of Zinc of the prepared nanomaterials. Also, these materials are termed as soft ferrites due to low coercive field in hysteresis loop. A. Hassadee et al. [47] found increase in lattice parameter, decrease in magnetization and coercivity in Zinc substituted Cobalt nanoparticles. Solution combustion route was used to synthesize Cobalt Zinc Fe_2O_4 nanoparticles with variation in Zinc concentration by Ritu Rani et al. [48]. They found that lattice parameter increases as Zinc concentration in prepared samples increases while hyperfine field, coercivity, remanence and saturation magnetization decreases. $Co_{0.5}Zn_{0.5}Fe_2O_4$ nanoparticles was fabricated via two dissimilar synthesis techniques and found that change in average particle size whereas both confirm single phase spinel structure. The magnetic properties vary conversely case of both synthesis routes. Hence, it shows that magnetic properties and morphology of $Co_{0.5}Zn_{0.5}Fe_2O_4$ nanoparticles could be controlled via selection of synthesis technique [49].

1.17 Aims and Objective

The objective of this thesis is to:

- Synthesis of Cobalt-Zinc ferrite nanoparticles using coprecipitation technique.
- Effect of annealing on Co-Zn ferrite nanoparticles.
- To study annealing effects on physical properties.
- To study annealing effects on magnetic properties.
- To investigate annealing effects on optical properties.
- Annealed Cobalt Zinc ferrite nanoparticles have been investigated by means of:
    - XRD, SEM, EDX, XRF, VSM and UV spectrometer.

CHAPTER 2 – EXPERIMENTAL TECHNIQUES

2.1 Introduction

For the investigation of different properties of ferrites, certain techniques have been used for their analyses. Different techniques give different information about the material i.e.; structure, morphology and composition. The experimental techniques used in this work are:

- X-Ray Diffraction (XRD)
- Scanning Electron Microscope (SEM)
- Energy Dispersive X-Ray Spectroscopy (EDX Or EDS)
- X-Ray Florescence (XRF)
- Vibrating Sample Magnetometer (VSM)
- UV Spectrometer

The crystallinity and phase of synthesized ferrite nanoparticles has been conceded by XRD. The morphology of ferrites has been determined by SEM. Presence of elements and the contents of each element in the synthesized ferrites have been explored by EDX. The composition of ferrites has been examined using XRF. The spinel ferrites have shown remarkable enhancement in magnetic hysteresis moment; which have been investigated using VSM. The tailoring in energy band gap by increasing values of annealing temperature has been confirmed by UV spectrometer. Short description of the experimental techniques is discussed in this chapter.

2.2 Structural Analysis

The structural analysis provides information about size, shape and structure of the material. The structural analysis of synthesized ferrite nanoparticles have been carried out using XRD.

2.2.1 X-Ray Diffraction (XRD)

XRD is one of primary tool that is used for the analysis of crystalline structure of material. The structural analysis of new materials or chemical identification of any material can carried out using XRD. This is non-destructive technique, which provides information about structural related parameters such as lattice constant, X-ray density, measured density and porosity. The XRD facility has been availed on Stoe, Model θ_θ diffractometer to find out phase structures of the

prepared compounds. The beam is focused and sharpens by using the collimators. The monochromatic focused electron beam is obtained by using filters. The sample has been used in powdered form, which has been placed in a plate shape sample holder made of Aluminum. The powder of each sample has been placed one by one. The monochromatic beam of X-rays CuK_{α} (λ=1.5406 Å) radiations at room temperature has been generated at a point and the intensity of the diffracted beam has been detected with a counter. The X-rays pattern has been obtained for each composition by changing the angle 2θ from 10°C - 80°C by step size of 0.04 degree per second. XRD peaks have been investigated through X'Pert HighScore software for identification and comparison [60]. The investigation of X-rays line broadening has been carried out by Debye-Scherrer formula (eq 4.1) subsequent to instrumental broadening.

X-rays are mostly included in electromagnetic radiations. X-rays usually preserve 0.5 Å - 2.5Å wavelength range, which is comparable to the interatomic spacing in solids [50]. The inelastic excitations of the core electrons are responsible for the production of X-rays in the atoms of target. For metal targets, the deceleration of fast moving electrons can also produced X-rays. The characteristic X-rays are obtained by first X-rays production process while second gives broad continuous spectrum [51]. In crystallographic point of view, planes have specific d-spacing with different orientations each with its own spacing in a crystal. When a radiation falls on a series of parallel planes which are equally spaced at a distance d then the path difference between the planes is 2dsinθ for all the reflected rays. This is the statement for Bragg's law. For constructive interference, only occurs for certain values of θ are entertained, the path difference for this is equal to n time's wavelength, i.e.

$$2d\sin\theta = n\lambda \qquad (2.1)$$

This is called Bragg's equation [52]; where λ is the wavelength, d is the spacing and n is an integer as shown in Figure 2.1. Equation 2.1 shows when $\lambda \leq 2d$ then reflection can only occur. This is why we can't use visible light [51].

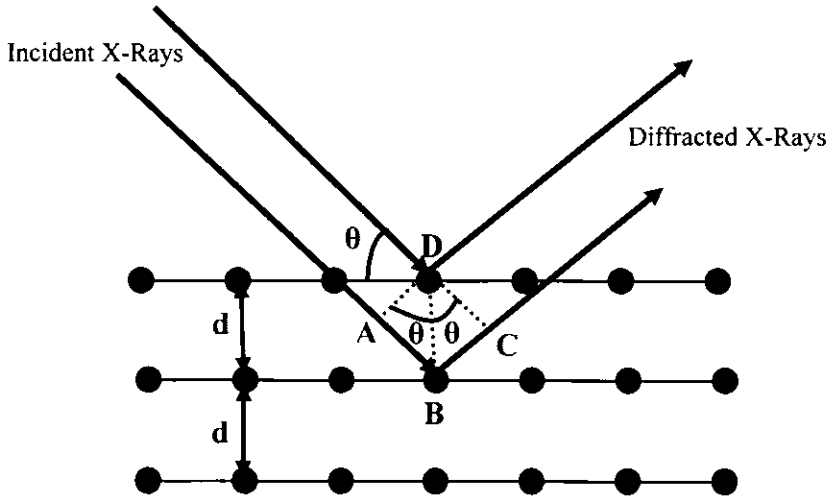

Figure 2.1: Diffraction of X-Rays.

The X-rays diffraction can be performed by following three methods based on Bragg's law:

- Rotating-crystal method
- Powder method
- Laue method

As samples in current work are in powder form, therefore, only brief description of powder route has been discussed here.

Powder method is very useful in finding crystal structure of powdered specimen. It is very reliable especially for small size single crystal. The crystal structure and grain size are easily be analyzed by powder method as single crystals are not required [51]. In powdered method, the specimen is grinded to a very fine powder and then put in a rectangular plate shape sample holder made of Aluminum or glass. Monochromatic X-rays beam is incident upon fine powdered specimen. Each particle of the powder is a tiny crystal oriented at random with respect to the incident beam. Let us consider one particular reflection of the radiation. The orientation of some of the particles of the powdered specimen makes the correct Bragg's angle for reflection at some (hkl) planes. Diffracted beam formed from one of the plane is shown in Figure 2.2 (a). When this plane is rotated about the incident beam by keeping angle θ constant, then the reflected beam will travel over the surface of a cone as shown in Figure 2.2 (b).

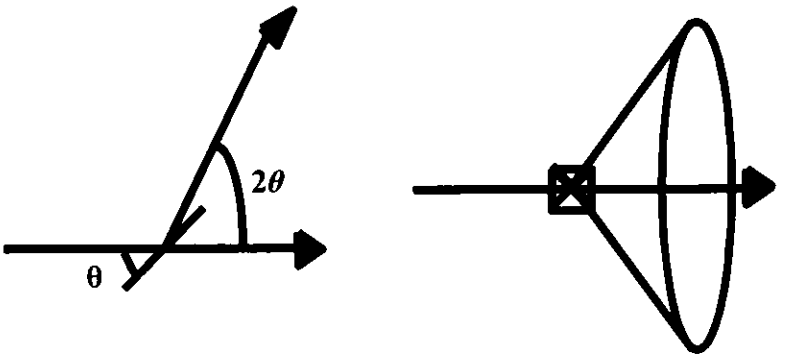

Figure 2.2: (a and b) Dependence of angle in Bragg's Law.

Due to many possible orientations in large number of crystal particles, this rotation is equivalent to these orientations because some of the particles satisfy Bragg's angle with the incident beam. We can easily calculate the interplanner spacing d if θ and λ of the measured diffraction line are known. For high-resolution data analysis, the diffractometer is very efficient.

TH 9435

2.3 Morphological Investigations

Morphology of prepared nanoparticles has been studied by means of Scanning Electron Microscope.

2.3.1 Scanning Electron Microscope (SEM)

SEM is a versatile characterization technique used for surface imaging and compositional mapping. SEM uses focused electron beam to generate a variety of signals that gives information about various parameters like morphology, microstructure, chemical composition, texture, orientation, crystalline structure and size of particles. SEM of synthesized samples have been done using Model Joel, JSM 6490A. As ferrites have high resistivity, therefore, the prepared samples have been sputtered by Gold coating in custom made setup assembly.

Typical SEM got essential components including electron gun, power supply, cooling system, electron lenses, detectors, vacuum system, sample chamber, vibration free floor, visual display monitors and room free of ambient magnetic and electric fields as shown in Figure 2.3. For

generation of a variety of signals at specimen, SEM uses high-energy focused electron beam (electron < 0.01mm in diameter) [53].In this system, Tungsten filament serves as a source to generate electrons upon heating. These electrons are focused toward anode. Voltage difference is created between filament and the anode to move the electrons down the column. This voltage differences is termed as accelerating voltage, which is, varied between 2 to 40 kV.

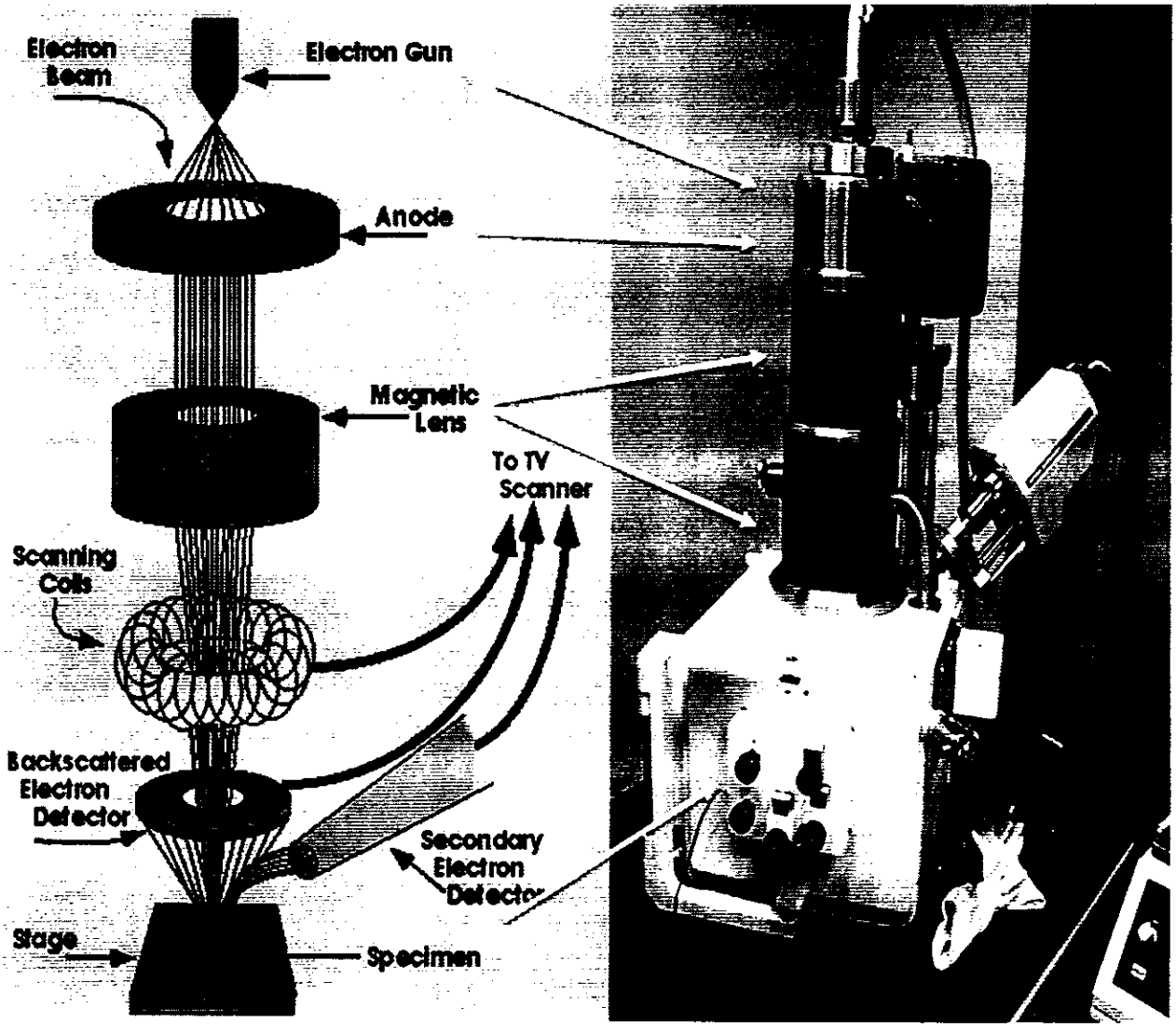

Figure 2.3: Comparision with setup diagram of SEM.

By electromagnetic lenses, the electron beam is condensed and focused. Main feature of two condenser lenses is to control the number of electrons striking the specimen and the spot size.

The objective lens or third condenser lens is used to focus electron beam on specimen surface. This lens is consisting of stigmator and deflecting coils. The forth and back movement of the electron spots and correction in irregularities is controlled by deflection and stigmator coils, respectively. This process is mainly used to minimize the losses in the resolution of SEM.

In SEM, the focused electron beam interacts with the sample to generate various signals, such as secondary electron, backscattered electrons and characteristic X-rays. These signals which are detected by the detectors form images of the sample (Figure 2.4). The low energy electrons are detected by the secondary electron detector providing a predominantly topographical image. The backward scattered electrons of very high energy are detected by back scattered electron detector, which points about the differences in atomic number of a sample. The liquid nitrogen cooled x-ray detector crystal is also a part of SEM that detects the emitted x-rays and analyzes the elemental content of a sample.

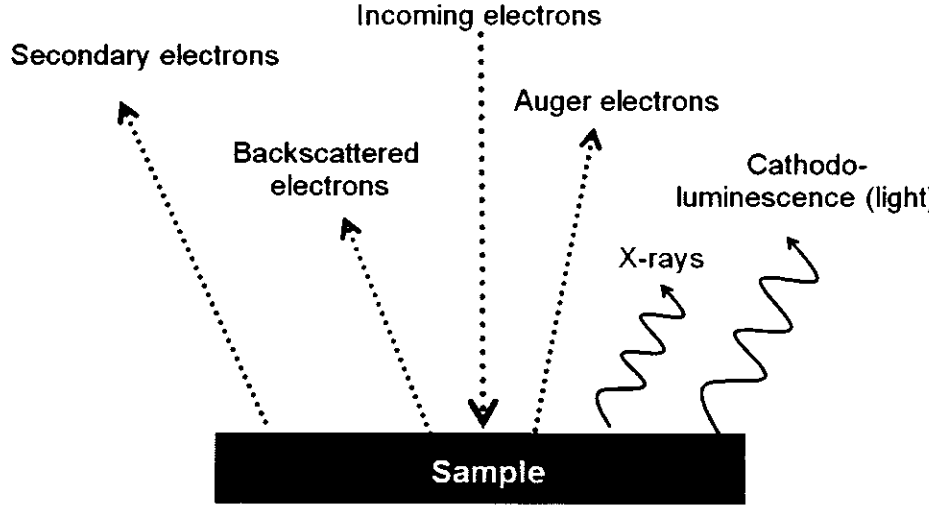

Figure 2.4: Working principle of SEM.

SEM is very useful as high values of magnification and exceptional focusing depth can be accomplished (Figure 2.3). Images obtained from SEM can also helpful in analyzing elemental composition using EDS or EDX.

2.4 Compositional Analysis

The compositional and chemical investigation of synthesized samples has been carried out by Energy Dispersive X-ray Spectroscopy (EDX) and X-Ray Fluorescence (XRF).

2.4.1 Energy Dispersive X-ray Spectroscopy (EDX)

Energy Dispersive X-ray Spectroscopy (EDX or EDS) is one of the analytical techniques which are used for compositional analysis of material. In EDX, the spectroscopic data are plotted as a graph of counts vs. energy. EDX characterization has been performed through Philips XL30ESEM containing EDAX microprobe for chemical identifications at 12KV; outfitted with a window for the detection of light elements. The chemical composition and contents of the chemicals have been analyzed by EDX spectrums. EDX characterizes the sample by interaction of matter and electromagnetic radiation. Then this is analyzed by the x-rays emitted through matter. As every element has distinctive atomic structure, therefore, permits x-rays to identify one elemental atomic structure to another.

For stimulating the emission of characteristic X-rays, high energy beam is bombarded to the sample which is subjected to study. The atom in at rest contains ground state electrons with discrete energy levels around nucleus. The incident beam excites the electron from inner shell which forms an electron hole pair in the atomic structure. This hole is filled from an outer shell electron whereas excess energy is released by that specific electron is released in X-ray form. These rays are released in such a way that they create spectral lines which are highly specific to individual elements and are applicable in analyzing the composition of samples. Morphological features seen in the SEM image are easily analyzed for elemental composition using EDX because experimental setup of EDX is in correspondence with SEM.

2.4.2 X-Ray Fluorescence (XRF)

XRF is non destructive chemical analysis characterization tool and is used for compositional analysis of the material. This facility has been availed using Model Jeol, Japan JSX3201M, with counting rate of 25266 counts/sec. XRF is basically emission of characteristic X-rays from material which is excited by bombardment of high energy X-rays or gamma rays. XRF

method depends on the interaction of electron beams and X-rays with the material, similar to SEM or EDX.

When a primary X-ray excitation source from an X-ray tube or a radioactive source strikes a sample, the X-ray can either be absorbed by the atom or scattered through the material. This ray is absorbed by the atom by transferring all of its energy to an innermost electron. When the primary X-ray had sufficient energy, then vacancies can be created by the ejection of the electrons from the inner shells giving birth to an unstable condition for atom. For the stability of atom, the electrons from the outer shells are transferred to the inner shells by giving off a characteristic X-ray. The energy of this characteristic X-ray is the difference between the two binding energies of the inner and outer shells. The emitted X-rays produced from this phenomenon are called XRF and the spectrometry used for of detecting emitted X-rays is called XRF Spectrometry. Innermost shells such as K and L shells are mostly involved in XRF detection. A typical X-ray spectrum from an irradiated sample will display multiple peaks of different intensities.

2.5 Magnetic Properties

The improvement in magnetic properties with applied magnetic field of the nanoparticles has been explored via vibrating sample magnetometer.

2.5.1 Vibrating Sample Magnetometer (VSM)

VSM is an instrument utilized for the measurement of moment or magnetization of the materials. The magnetic measurements of nanoparticles have been performed by means of magnetometer VSM, Model BHV-50, Riken Denshi Co. Ltd. Japan. The plots of magnetization M verse applied magnetic field H has been achieved at room temperature with field ranging between -8,000 Oe – 8,000 Oe using VSM which exhibits a clear hysteretic behavior. When the material is placed in uniform magnetic field, a dipole moment induced in the sample. An electrical signal is induced in stationary pick-coils when sample undergoes the sinusoidal motion which is proportional to magnetic moments, vibration frequency and amplitude. VSM displays the magnetic moment in emu units.

VSM operates by placing the material in a constant magnetic field in its first step. This magnetic field will magnetize the materials with the alignment of magnetic domains and individual magnetic spins through magnetic field. Magnetization of the material will be large for stronger constant field. The dipole moment will create a magnetic field around sample when sample has certain motion, i.e.; move up and down. This magnetic field will vary with time and is easily detected via set of pick up coils. This changing field originates an electric field in pick up coils, stated by, Faraday's law of electromagnetic induction. The current produced in the sample is proportional to its magnetization. Hence, greater is the induced current, greater will be magnetization. The magnetization of the sample can be calculated by using monitoring and controlling software, which also give information that how magnetization is dependent on strength of constant magnetic field. VSM is consisted of components, such as electromagnet, sample holder, power supply, sensor coils, vibration exciter, pickup coil, amplifier and computer interface as shown in Figure 2.5 [9].

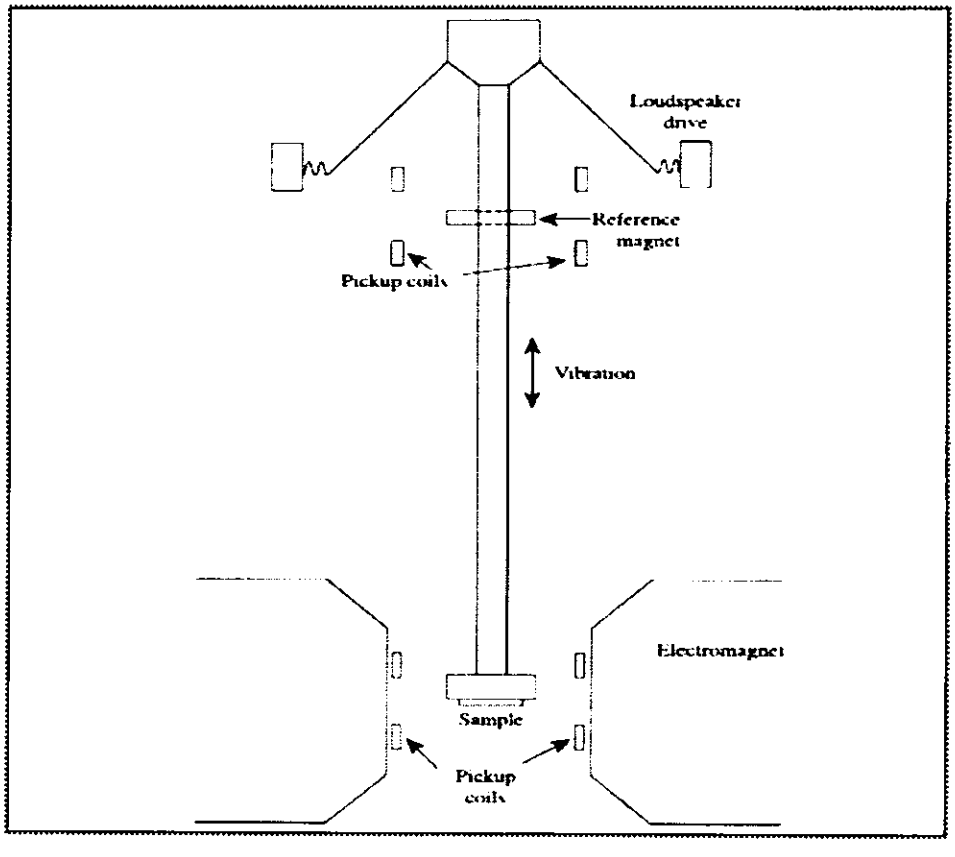

Figure 2.5: Schematic Diagram of Vibrating Sample Magnetometer [5].

The M-H loops at room temperature (Magnetization versus applied magnetic field) have been obtained by Faraday's law of induction that is due to induced Emf generated by change in flux. The constant magnetic field use to magnetize the sample is generated by water cooled electromagnets in conjunction with power supply. The magnetic properties are investigated using VSM by taking following steps:

- The strength of constant field is set.
- Place the sample on the holder.
- Vibration of sample to produce flux.
- Translation of signal from probe to moment of sample.
- The strength of constant magnetic field changed to new value.
- Don't take readings/data during this translation.
- The strength of constant magnetic field attains new value.
- The signal from probe again turns to value for magnetization of sample.
- The constant field varies along given range.
- Plot of magnetization vs. magnetic field strength is generated.

2.6 Optical Properties

The study of percentage diffuse reflectance and the optical band gap of nanoparticles have been examined using Ultraviolet (UV) spectrometer.

2.6.1 UV Spectrometer

For the investigation of optical properties versatile Lambda 950 doubled beam spectrometer has been used, operating in the Ultraviolet (UV), Visible (Vis) spectral ranges. This spectrometer is a double monochromator that operates in near infrared region. The durability of optical mechanism is maintained by coating of silica. Characteristic optical Lambda 950 spectrometer features are depicted in Figure 2.6. The diffused reflectance spectra are obtained within wavelength range of 400 nm – 800 nm at room temperature. The energy band gap of the material is calculated using reflectance spectra and standard relations (eq 4.6 and 4.7). For direct

band gap materials, absorption coefficient "α^2" is used. The energy band gap has been easily obtained by extrapolation of linear part of spectra towards x-intercept.

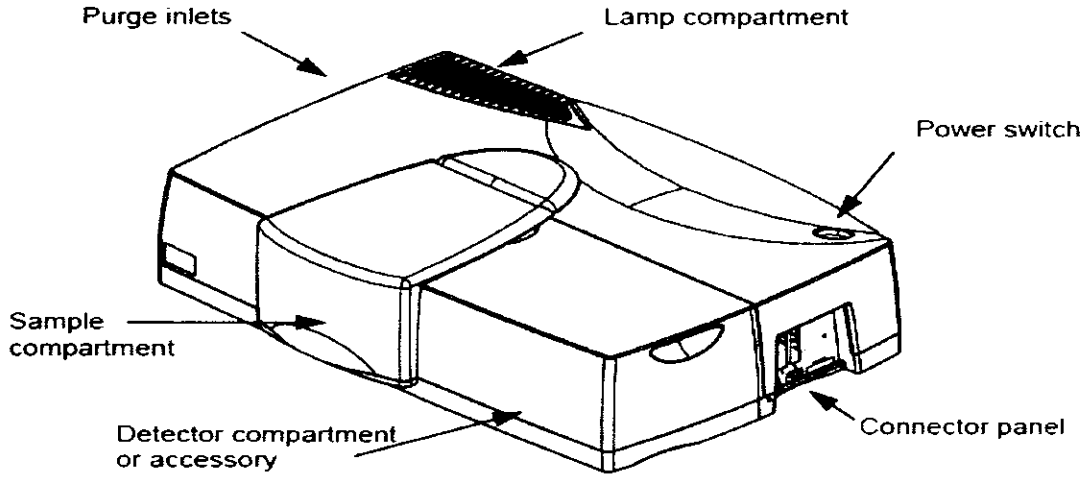

Figure 2.6: Features of Lambda 950 UV spectrometer.

Optical spectrometer contains four windows with sealed whole optical compartment. Moreover, the sample partition is sealed by windows from detectors in addition to optical compartment. Hence, these windows are used to protect the optical components of the spectrometer from fuming, dust and hostile samples. Main sources of light in spectrometer are Halogen Lamp (HL) and Deuterium Lamp (DL) that operate in Visible Near-Infrared (Vis-NIR) region and UV region, respectively. Hence, the working range lies in 175 nm - 3300 nm. This optical spectrometer takes scans from higher wavelengths to lower ones.

The schematic diagram of optical spectrometer is shown in Figure 2.7. Source mirror M1 reflects radiations onto mirror M2 for operating in Vis/NIR region. The collimated beam, depending on wavelength, either strikes NIR or UV-Vis grating. The spectrum is generated by the dispersion of radiation on the grating and exits slit reveal high spectral purity with extremely low stray radiation content. The dark signal is created at detector when no radiations reached to detector due to dark segment in the beam's path. Lead Sulfide "PbS" detector is used for NIR wavelength range and Photo-Multiplier "PM" is for UV-Vis wavelength range. Slit width is highly significant for beams width. The monochromator slewing detector's change is throughout automatic.

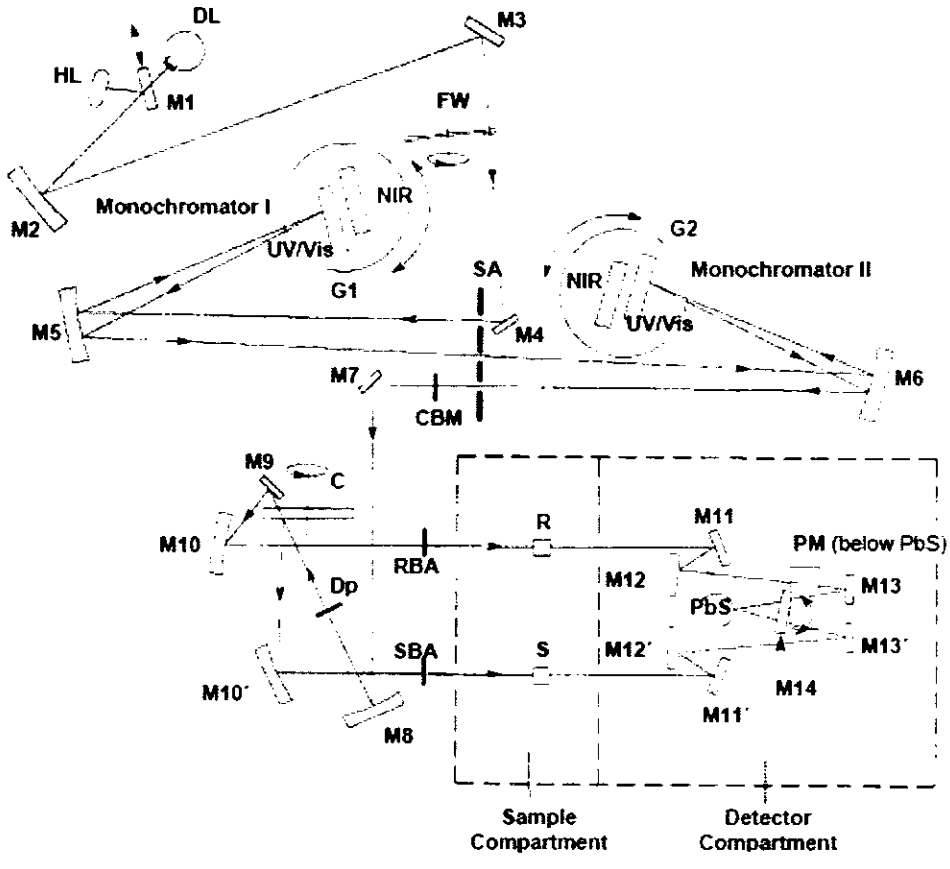

Figure 2.7: Schematic diagram of Optical Spectrometer.

Reflectance accessory of spectrometer composites of two fundamental components; firstly, an integrating sphere (150mm) and, secondly is optics chamber. The integrating sphere acts as internal diffuse reflectance accessory which loads directly into detector compartment of spectrometer. The principle working of integrating sphere is to integrate the light beams on the samples. The optics chamber contains the transfer optics that guides the instrument sample and reference beams to their respective entrance ports on the integrating sphere. The integrating sphere is 150 mm in a diameter and is constructed of a highly diffuse reflecting material. There are two detectors embedded in the internal walls of the integrating sphere; a Lead Sulfide (PbS) detector and an extended range Photo-Multiplier Tube (PMT). During reflectance phenomenon, the integrating sphere collects and detects the radiation input by the spectrophotometer beams and relays the information to the UV WinLab software.

CHAPTER 3 – SYNTHESIS TECHNIQUES

3.1 Introduction

Synthesis techniques are highly significant for the fabrication of nanostructures. The synthesis of nanomaterials has been maturing with new postulates and procedures that have been introduced on daily basis. There are several synthesis techniques that can be used for the preparation of nanostructures. The synthesis of nanostructures has been classified into two following synthetic approaches. i.e;

- Top-Down Approach
- Bottom-Up Approach

One can imagine that new synthetic strategies will be evolved in the future as the requirement for specific size and shape of the material increases. Both the approaches give significant results in order to use them properly and carefully.

3.2 Methods of Preparation

In bulk form, the ferrites are prepared through solid state reaction [8].There are many techniques for the synthesis of ferrite nanoparticles which includes Matrix Isolation, Sol-Gel Method, Coprecipitation Method, Evaporation Condensation and Hot Sparing Method. The synthesis of nanoparticles is mostly carried out by two distinct methods which are classified as:

- Physical Method
- Chemical Method

3.2.1 Physical Methods

In physical methods, the formation of nanoparticles has been carried out by decomposition of bulk material to nanoscale. Some of the characteristics of physical methods are;

- Subdivision of bulk metals via mechanical crushing or pulverization of bulk material.
- Arch discharge between metal electrodes.
- Metallic nanoparticles produced have large size and distribution.

3.2.2 Chemical Methods

In chemical methods, the fabrication of nanoparticles has been brought at atomic scale. The chemical methods have numerous characteristics such as:

- Nanoparticles have narrow size distribution.
- Easy to operate
- Based on reduction of metal ions.
- Decomposition of precursor for the formation of atom followed by aggregation of atoms.

The methods which can be used for the preparation of nanomaterials by using different synthetic approaches have been shown in Figure 3.1.

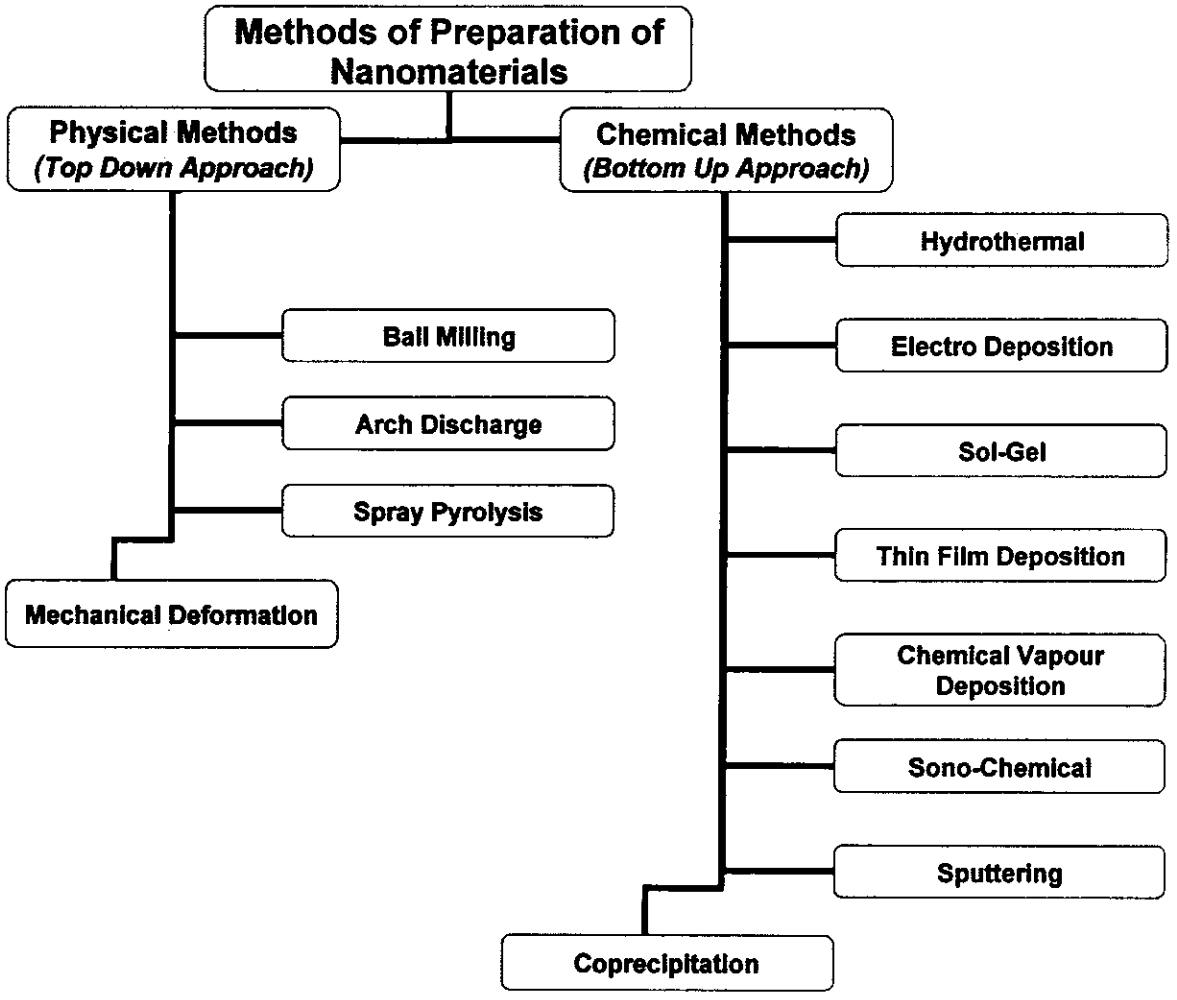

Figure 3.1: Flow chart for different synthesis approaches.

Both of these synthesis approaches give same results whether chemical method (bottom-up approach) or physical method (top-bottom approach) is used as shown in Figure 3.2.

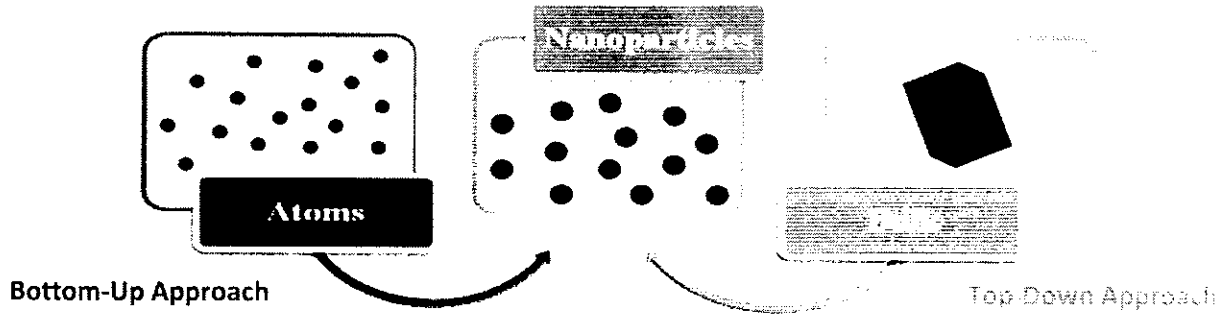

Figure 3.2: Comparison of two approaches of synthesis.

Though many methods are available, the choice of a particular method depends on the type of materials, the geometry required and also the scale at which the product has to be produced. **In current dissertation, chemical coprecipitation method *(bottom-up approach)* has been used for synthesis of ferrite nanoparticles so it has been described in detail only.**

3.3 Chemical Coprecipitation Method

Chemical coprecipitation is the most useful and easiest technique for the synthesis of $Co_{1-x}Zn_xFe_2O_4$ ($x = 0.5$) nanoparticles. Chemical coprecipitation method has been easy to operate due to numerous characteristics such as low temperature, broad size distribution, achievement of well disperse nanoparticles, concentration of metal salts and reducing agent affect the properties of nanomaterials and the precipitating agent has no significant effect on morphology of nanomaterials.

In chemical coprecipitation method, aqueous salt solutions of reactants have been mixed to produce precipitation of insoluble substance by exceeding the solubility limit. The size of nanoparticles has been controlled by optimizing different synthesis parameters such as pH value, concentration of dopants and reaction time. The prepared samples have been annealed at various temperatures to improve their physical properties. High pH values have been used where large production yields have been expected [54].

3.3.1 Principle of Reaction

The trivalent Fe^{3+} and bivalent metal M^{2+} aqueous solutions form fine ferrites nanoparticles. The bivalent metal M^{2+} can be Co^{2+}, Fe^{2+}, Zn^{2+} and Mn^{2+} cations. The coprecipitation takes place in two steps.

- Coprecipitation step
- Ferritisation step

3.3.1.1 Coprecipitation Step

In first step, solid hydroxides of metals in the form of colloidal particles have been obtained by the coprecipitation of metal cation in alkaline medium. For the case of $Co_{1-x}Zn_xFe_2O_4$ nanoparticles, the reaction is as follows,

$$(1-x)CoSo_4.7H_2O + (x)Zn(No_3)_2.6H_2O + FeCl_3.6H_2O + 8\,NaOH$$

$$\Downarrow$$

$$(1-x)Co(OH)_2.(x)Zn(OH)_2.2\,Fe(OH)_3$$

3.3.1.2 Ferritisation Step

In second step, the product has been subjected to heating in the precipitation alkaline solution to provide the transformation of solid solution of metal hydroxides to the $Co_{1-x}Zn_xFe_2O_4$ nanoparticles [55],

$$(1-x)Co(OH)_2.(x)Zn(OH)_2.2\,Fe(OH)_3$$

$$\Downarrow$$

$$Co_{(1-x)}Zn_{(x)}Fe_2O_4.nH_2O + (4-n)H_2O$$

Where n is integer.

The particular feature of the coprecipitation method as comparison to high temperature synthesis methods of the ceramics ferrites is that the product contains a certain amount of

associated water even after several hours of the heating in alkaline solution. In order to get rid of these water contents, this product has been placed in vacuum oven for overnight.

3.4 Synthesis Parameters and Their Influence on Properties of Nanoferrites

Synthesis parameters and equipments play very important role in synthesis of nanostructures. The variation in properties of these synthesis parameters can influence the properties of prepared nanostructure. For the preparation of Cobalt Zinc spinel ferrite nanoparticles, the required equipments and few synthesis parameters, their influence on the properties of ferrite nanoparticles have been discussed below. The equipment used for the preparation of spinel ferrites nanoparticles was digital balance, hydraulic press, die, boats and furnace.

3.4.1 Magnetic Stirring

The uniform mixing and heating of the solution is highly valuable for the synthesis of nanoparticles. These two parameters highly influence properties of the prepared samples for example size of particles etc. The solution of metal salts have been uniformly mixed and heated through magnetic stirrer for 45minutes. The temperature of the machine ranges from 50°C to 370°C. The stirring capacity ranged up to 15litres of solution. The maximum stirring power of machine is 30W.

3.4.2 Rate of Mixing Reagents

The rate of mixing of reagents plays a vital role in the size of the resultant particles. Chemical coprecipitation route composed on two processes; (i) nucleation (structure of centers of crystallization) and (ii) successive growth of particles. The size of particles and polydispersity of the particles have been determined by comparative rate of these processes. When nucleation rate is high and growth of particle is slow then less dispersed collides have been formed. The polydispered collides have been achieved by simultaneous growth of former particles and formation of new nuclei. This reflects dynamic change in reaction by rapid mixing of reagents. Hence, the formation of bigger nuclei could be possible only by slow addition of reagents than the rapid ones. Ferrite nanoparticles of chemically homogenous, smaller and less dispersed in size have been obtained via fast mixing of reagents in the reaction.

3.4.3 Effect of pH of Reaction

The precise measurement of pH value and temperature of the solution has been calculated using pH meter. The pH meter ranges pH value from -2 to 16 with accuracy ± 0.02 and temperature from -10°C to 105°C. The formation of spinel ferrites has been possible when the yield of ferrites grew. The pH value of the reaction has been increased from 6.8 - 8.6 followed by slight increase in yield of ferrites. The remarkable point is that further increase in pH value, i.e.; 12.5 - 14 leads to considerable growth of yield. The formation of spinel ferrites became short at high pH values. It has been observed that the synthesized Cobalt Zinc ferrite nanoparticles have been formed at optimal value of 11 - 12.5.

3.4.4 Effect of Reaction Temperature

Temperature is one of the important parameters for the synthesis of ferrite nanoparticles. The increase in temperature ranging 20°C - 100°C extensively causes the formation of ferrite nanoparticles. Different metals have different activation energy ΔE for the formation of ferrite nanoparticles. The ΔE has been calculated from kinetics of the formation reaction in 20°C - 100°C temperature. It has been estimated that the ΔE of Cobalt and Zinc goes in $E_{A\,(Co\text{-}ferrites)} > E_{A\,(Zn\text{-}ferrites)}$ manner. In current work, the reaction temperature of the solution has been kept at 70°C - 85°C.

3.4.5 Heating after Coprecipitation

The coprecipitation occurs in concentrated solution and it has no information about growth of particle size which has been caused in the system during long heating process. In our case, we heated the precipitates of Cobalt Zinc nanoparticles for 45min and dried the nanoparticles at 100°C for overnight.

3.4.6 Role of Anion

In coprecipitation solution, the type of anion effects the properties of particles obtained. For the coprecipitation of Cobalt Zinc ferrite nanoparticles, chlorides or nitrates salts have been used. So, for more equal conditions for all three metals, these metals ought to take in salts, nitrates or chloride form.

3.5 Chemicals for Synthesis of Cobalt Zinc Ferrite Nanoparticles

For the synthesis of Cobalt Zinc ferrite nanoparticles, Zinc Nitrate ($Zn(No_3)_2.6H_2O$), Cobalt Sulfate ($CoSo_4.7H_2O$), Iron Chloride ($FeCl_3.6H_2O$), Sodium Hydroxide (NaOH) and acetone have been used. The chemicals have been used without supplementary refinement. The aqueous solution of above chemicals has been prepared using distilled water as solvent, which has low conductivity.

3.6 Synthesis of Cobalt Zinc Ferrite Nanoparticles

Synthesis of $Co_{1-x}Zn_xFe_2O_4$ ($x = 0.5$) nanoparticles has been carried out via chemical coprecipitation technique. Appropriate molar ratios of Zinc Nitrate ($Zn(No_3)_2.6H_2O$), Cobalt Sulfate ($CoSo_4.7H_2O$) and Iron Chloride ($FeCl_3.6H_2O$) have been used for the preparation of $Co_{0.5}Zn_{0.5}Fe_2O_4$ nanoparticles. The molarities of Iron (Fe), Cobalt (Co), Zinc (Zn) and NaOH have been 0.02, 0.01, 0.01 and 0.15Mol in 100ml respectively. The pH value of $Co_{1-x}Zn_xFe_2O_4$ ($x = 0.5$) solution has been controlled from 11 - 11.5 by addition of 2M NaOH drop wise during stirring. Due to lack of partial oxidation of Iron-II compounds, ferric precursor is mostly used for synthesis of nanoparticles [56].

The use of NaOH as precipitating agent is one of the important aspects for the synthesis of ferrite nanoparticles. The morphology of ferrite nanopowders synthesized via coprecipitation route has been highly influenced by nature of precipitating agent. In the literature, Urea and Ammonia solutions had been used as precipitating agent [57], however, the use of NaOH in current studies offer numerous advantages as compared to Urea and Ammonia. For example, the Hydroxide ions has been formed when Urea experience hydrolysis reaction at temperature greater than 333K. Meanwhile, when precipitation is performed with NaOH besides NH_4OH, the resulting spherical shaped particles acquire comparatively narrow size distribution and good crystallinity [58]. In addition, since regardless of any morphology, the nanostructured ferrite materials resulting from the appropriate heat treatment consist of agglomerated particles. The morphological changes of the as-prepared nanopowders during the annealing process have been found to depend on their initial composition. Thus, while in the NaOH medium the transition-metal ions precipitate as hydroxides, in the presence of an Ammonia solution the coprecipitation occurs with the formation of transition-metal complexes incorporating the NH^{+4} ions [59].

Temperature is one the major parameter in synthesis of ferrites nanoparticles prepared via coprecipitation process. It has been seen that when metal ions are precipitated at room temperature, the amorphous intermediate compounds such as hydroxides or oxyhydroxides separate from the reaction solution [60]. Heat treatment at around 100°C has been required to digest the resulting precipitate in order to obtain the corresponding nanocrystalline ferrite materials. This post-process of thermal treatment can influence the size of the ferrite nanoparticles. In current work, the coprecipitation reaction has been maintained at 70°C - 75°C containing the metal precursors and the precipitating agent. The elevated temperature thus facilitates the immediate conversion of the hydroxo intermediates into nanocrystalline ferrites of single phase mixed metal oxides with spinel structure and good crystallinity. The salt impurities have been removed through washing the particles with distilled water repeatedly. Later on, the water washed particles have been dried at 100°C in vacuum oven for overnight.

3.7 Annealing Temperature of Cobalt Zinc Ferrite Nanoparticles

In order to see the effects of annealing on the crystallinity, morphology and physical properties, the prepared $Co_{1-x}Zn_xFe_2O_4$ (x = 0.5) nanoparticles have been annealed at various temperatures. The electric furnace has been used to anneal the synthesized $Co_{1-x}Zn_xFe_2O_4$ (x = 0.5) nanoparticles at 500°C, 650°C and 1000°C. The prepared Cobalt Zinc ferrite nanoparticles have been annealed for 7 hours.

3.8 Summary of Experimental Procedure for CoZn Fe_2O_4 Nanoparticles

$Co_{0.5}Zn_{0.5}Fe_2O_4$ nanoparticles have been synthesized using Zinc Nitrate, Cobalt Sulfate, Iron Chloride, Sodium Hydroxide and acetone. The pH value of solution has been maintained within range of 11-12 through usage of NaOH. In order to enhance the physical properties of Cobalt Zinc ferrite nanoparticles, the nanoparticles have been annealed at 500°C, 650°C and 1000°C. Many characterization techniques have been used for the investigation of structural, morphological, compositional, magnetic and optical properties of prepared $Co_{0.5}Zn_{0.5}Fe_2O_4$ nanoparticles using XRD, SEM, EDX, XRF, VSM and UV spectrometer. The detailed flow chart of experimental procedure has been shown in Figure 3.3.

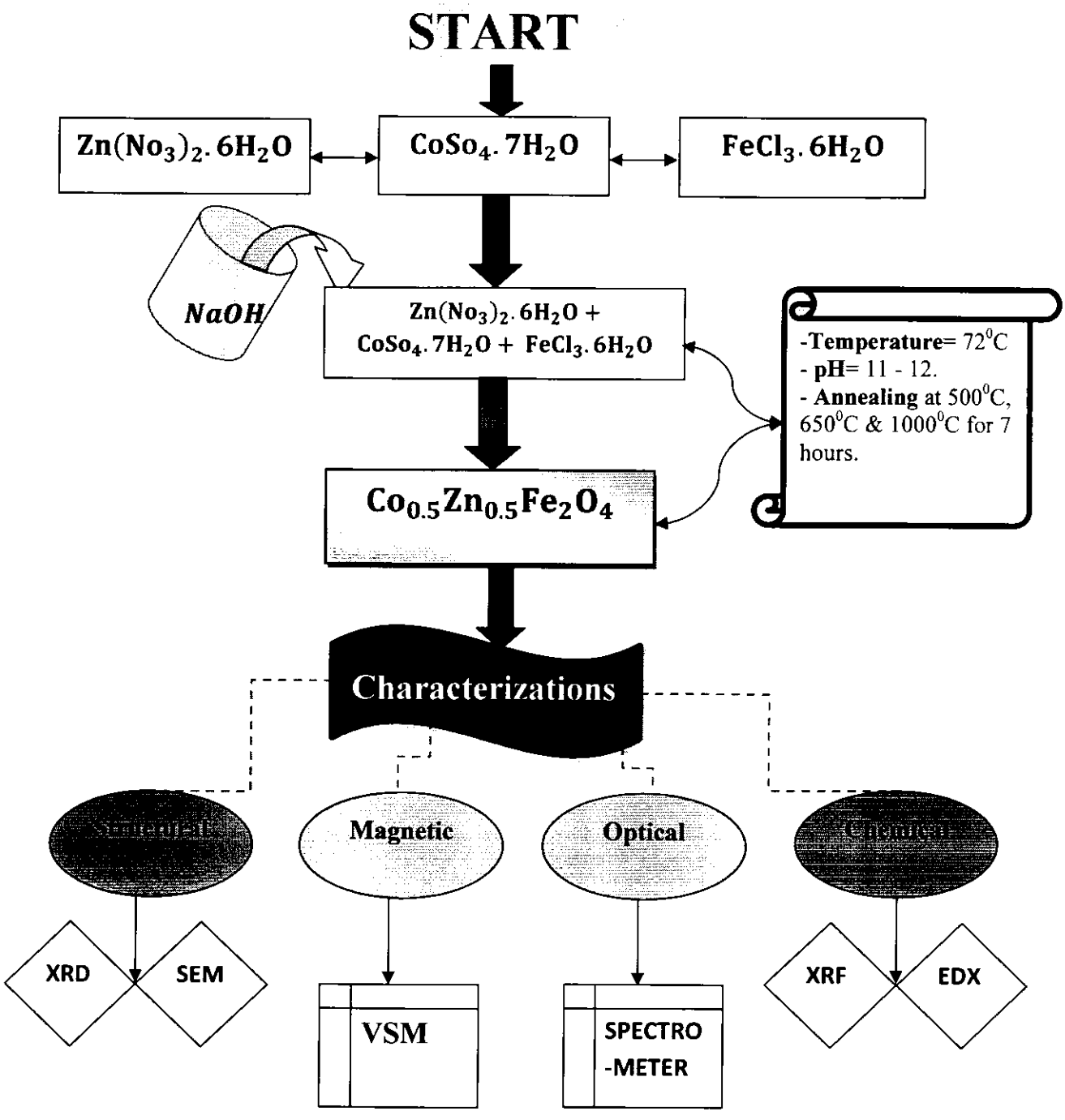

Figure 3.3: Flow chart of experimental procedure for CoZn ferrite nanoparticles.

CHAPTER 4 – RESLUTS AND DISCUSSION

4.1 Introduction

Many characterization techniques have been used for the investigation of diverse properties of ferrite nanoparticles. These characterization techniques provide different information such as structure, morphology, composition, magnetic and optical properties of prepared nanoparticles using XRD, SEM, EDX, XRF, VSM and UV spectrometer.

4.2 Structural Characterization

XRD has been used for the analysis of crystalline structure and structural analysis of prepared material. XRD peaks have been investigated through X'Pert HighScore software for the identification and comparison of doped ferrite nanoparticles [61]. The investigation of X-rays line broadening of X-rays has been carried out by Debye-Scherrer formula (eq 4.1) subsequent to instrumental broadening. The lattice constant, average crystallite size, measured density, x-ray density and porosity have been calculated through standard relations, described elsewhere [62, 63].

Figure 4.1 shows the XRD patterns of prepared material. It has been evident from the Figure 4.1, all the prepared samples of $Co_{1-x}Zn_xFe_2O_4$ ($x = 0.5$) nanoparticles with varying annealing temperature exhibit single phase spinel structure lacking of additional impurity phases. One extra peak appears 32^o in sample annealed at 650°C which is of zincite. The XRD peaks coincide quite well with reflection of Cobalt Zinc ferrite nanoparticles found with the published work [64, 65]. By using d-spacing and respective (hkl) parameters lattice constant 'a' has been calculated. Analysis of XRD peaks confirmed the formation of cubic spinel structures, as main peaks are indexed to standard spinel structures of XRD patterns. The XRD peaks (111), (311), (222), (400), (331), (422), (511), (440) and (531) are cubic unit planes that reflect cubic spinel structure and the plane (311) shows exact spinel phase. The diffraction patterns of $Co_{1-x}Zn_xFe_2O_4$ ($x = 0.5$) nanoparticles prepared by coprecipitation technique at various annealing temperatures 500°C, 650°C and 1000°C have been shown in Figure 4.1.

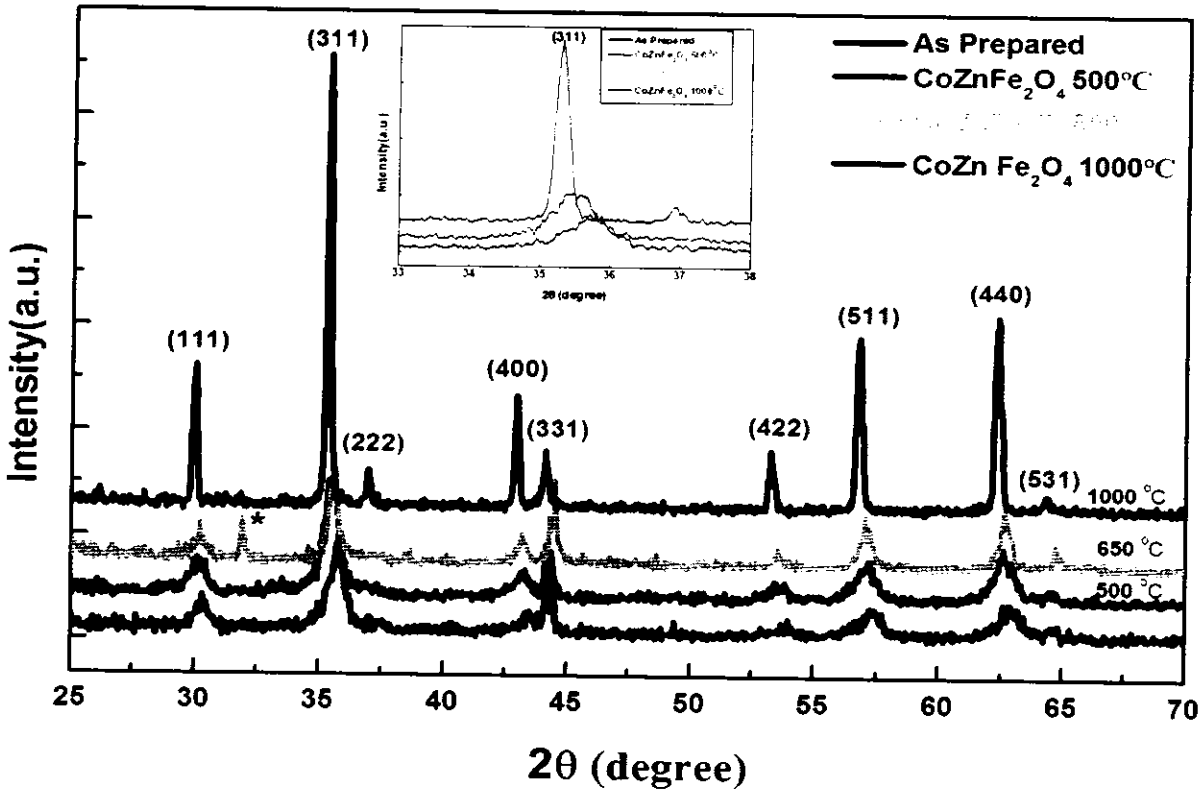

Figure 4.1: XRD pattern of CoZn ferrite nanoparticles annealed at various temperatures.

It has been observed that the width of diffraction peaks contracts as the annealing temperature of prepared samples increases. This decrease is due to increase in grain size of ferrite nanoparticles. The observed narrower peaks indicate that crystallite size increases with increase in annealing temperature. The characteristic parameters of $Co_{1-x}Zn_xFe_2O_4$ (x = 0.5) samples annealed at 500°C, 650°C and 1000°C temperatures have been summed up in Table 2.

4.2.1 Crystallite Size

The average crystalline size of samples has been calculated using Debye-Scherrer formula;

$$D_{XRD} = \frac{0.9\lambda}{\beta cos\theta} \qquad (4.1)$$

where 'λ' represents wavelength of X-Ray used in Å, 'θ' represents Bragg's angle, 'β' is in radians which is basically Full Width at Half Maxima (FWHM) and crystallite size by 'D_{XRD}' in Å. All the peaks of the planes of spinel structure are correspondent to line broadening of XRD peaks [66]. In current work, the crystallite size ranged within 160 Å - 417 Å.

The prepared $Co_{1-x}Zn_xFe_2O_4$ (x = 0.5) nanoparticles showed cubic structure with Fd-3m space group. Figure 4.2 clearly shows that lattice parameter of prepared nanoparticles increases with increase in annealing temperature. XRD analysis confirm regular indexed peaks of prepared annealed samples which indicate that crystallite size of particle increases as annealing temperature of samples increases and intense diffraction features became stronger due to growth of gain size. Also, these parameters have been significantly influenced by the ionic radii of contents used of preparation of nanoparticles. The increase in lattice parameter is due to large ionic radii of Zinc (Zn^{2+} - 88pm) in contrast with Cobalt (Co^{3+} - 83.8pm). The observed parameters in current work are good accord with numerous other studies where larger metal ions are substituted with smaller ones [67].

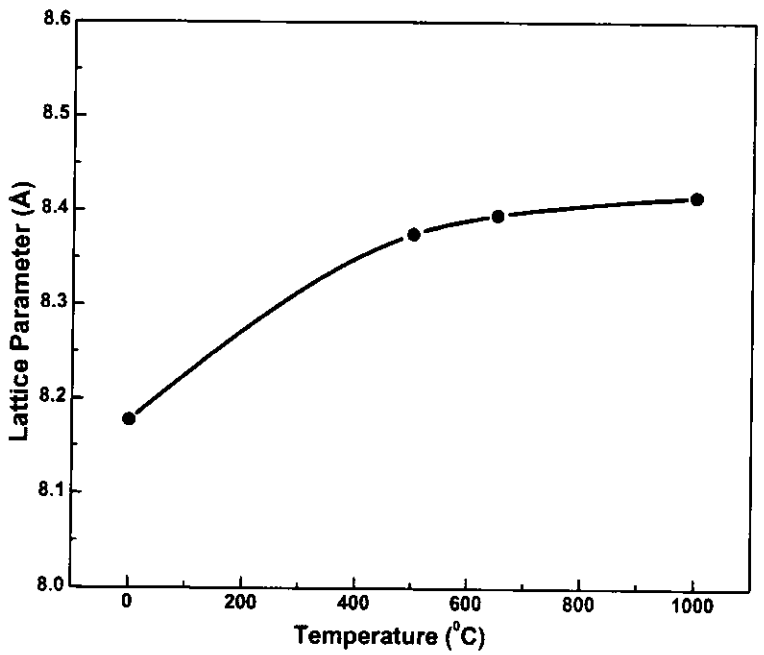

Figure 4.2: Plot of lattice parameter verses annealing temperature.

For further investigations of structural properties of $Co_{1-x}Zn_xFe_2O_4$ (x = 0.5) nanoparticles; measured density, X-Ray density and porosity of as prepared samples have been calculated.

4.2.2 Measured Density

The measured density 'ρ_m' of the annealed $Co_{1-x}Zn_xFe_2O_4$ (x = 0.5) nanoparticles have been calculated from the following relation [68]:

$$\rho_m = \frac{m}{\pi r^2 h} \qquad (4.2)$$

Where 'm' is mass and 'r' is the radius and 'h' is the height of prepared samples. ρ_m decreases with the increase in annealing temperature of ferrite nanoparticles. This trend appears due to different atomic masses of Cobalt and Zinc which in result affects the density of the nanoparticles. The decrease in density of prepared nanoparticles is also because of increase in volume of unit cell.

4.2.3 X-Ray Density

Figure 4.3 shows X-ray density 'ρ_x' as function of annealing temperature of synthesized $Co_{1-x}Zn_xFe_2O_4$ (x = 0.5) nanoparticles. The 'ρ_x' of the as prepared samples have been using following relation [41]:

$$\rho_x = \frac{8M}{Na^3} \qquad (4.3)$$

Where 'M' represents molecular mass of samples, 'N' is Avogadro's number; 'a' is the lattice parameter and 8 represents that each cell has 8 formula units.

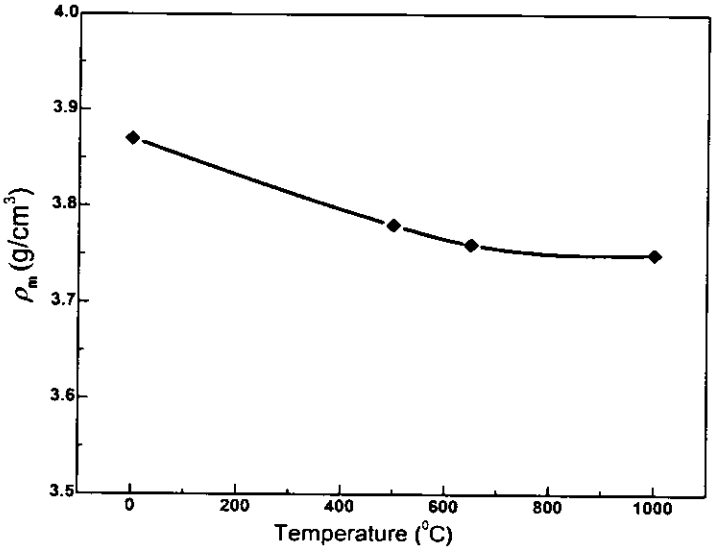

Figure 4.3: Plot of X-ray density verses annealing temperature.

Table 2 and Figure 4.3 indicate that ρ_x decreases from 3.87 g/cm^3 to 3.75 g/cm^3 with increasing values of annealing temperature from 0°C to 1000°C of the prepared $Co_{1-x}Zn_xFe_2O_4$ (x = 0.5) nanoparticles. This is due to different atomic masses of Cobalt and Zinc which consequently affects the density of nanoparticles due to increase in volume of prepared samples.

4.2.4 Porosity

Table 2 indicates that the porosity of $Co_{1-x}Zn_xFe_2O_4$ (x = 0.5) nanoparticles is significantly affected by annealing temperature. The porosity of prepared nanoparticles has been estimated using following relation:

$$P = 1 - \frac{\rho_m}{\rho_x} \qquad (4.4)$$

Table 2 shows that the porosity decreases as annealing temperature of prepared $Co_{1-x}Zn_xFe_2O_4$ (x = 0.5) nanoparticles increases from 0°C to 1000°C. The porosity of prepared nanoparticles decreases due to increase in particle size and surface area. This trend is also due to increase in grain boundaries of nanoparticles with increase in annealing temperature. The decrease in porosity shows that the prepared nanoparticles have been becoming more crystalline with increase in annealing temperature. Hence, the smaller grains produce large number of grain boundaries.

4.3 Morphological Study

The morphology of annealed $Co_{1-x}Zn_xFe_2O_4$ (x = 0.5) nanoparticles have been studied by means of SEM. SEM provides information about morphology and grain size of particle. Figure 4.4 shows the SEM images of prepared samples. The micrograph taken from SEM displayed single phase structures. SEM micrographs did not showed any other phase due to interdiffusion between phases. On the other hand, many clusters of agglomerations of ferrites have been expected which are commonly found in such ferrite nanoparticles [69, 70]. However, the samples look to have spherical nanosized grains.

Figure 4.4 indicate that the average particle grain size have been experienced between 20nm-130nm for prepared $Co_{0.5}Zn_{0.5}Fe_2O_4$ nanoparticles. In current work, uniform distribution of nanoparticles has been observed which reflects the significance of coprecipitation technique used for preparation of ferrite nanoparticles. Figure 4.4 shows that the grain size of nanoparticles significantly increases as function of annealing temperature. The increase in grain size can be understood on the basis of grain boundaries. With the increase in annealing temperature, pores have been observed on grain boundaries. SEM of $Co_{1-x}Zn_xFe_2O_4$ (x = 0.5) nanoparticles annealed at 500°C (Figure 4.4 b and b'), 650°C (Figure 4.4 c and c') and 1000°C (Figure 4.4 d and d') temperature have been taken within range of 5,000 - 100,000 magnifications.

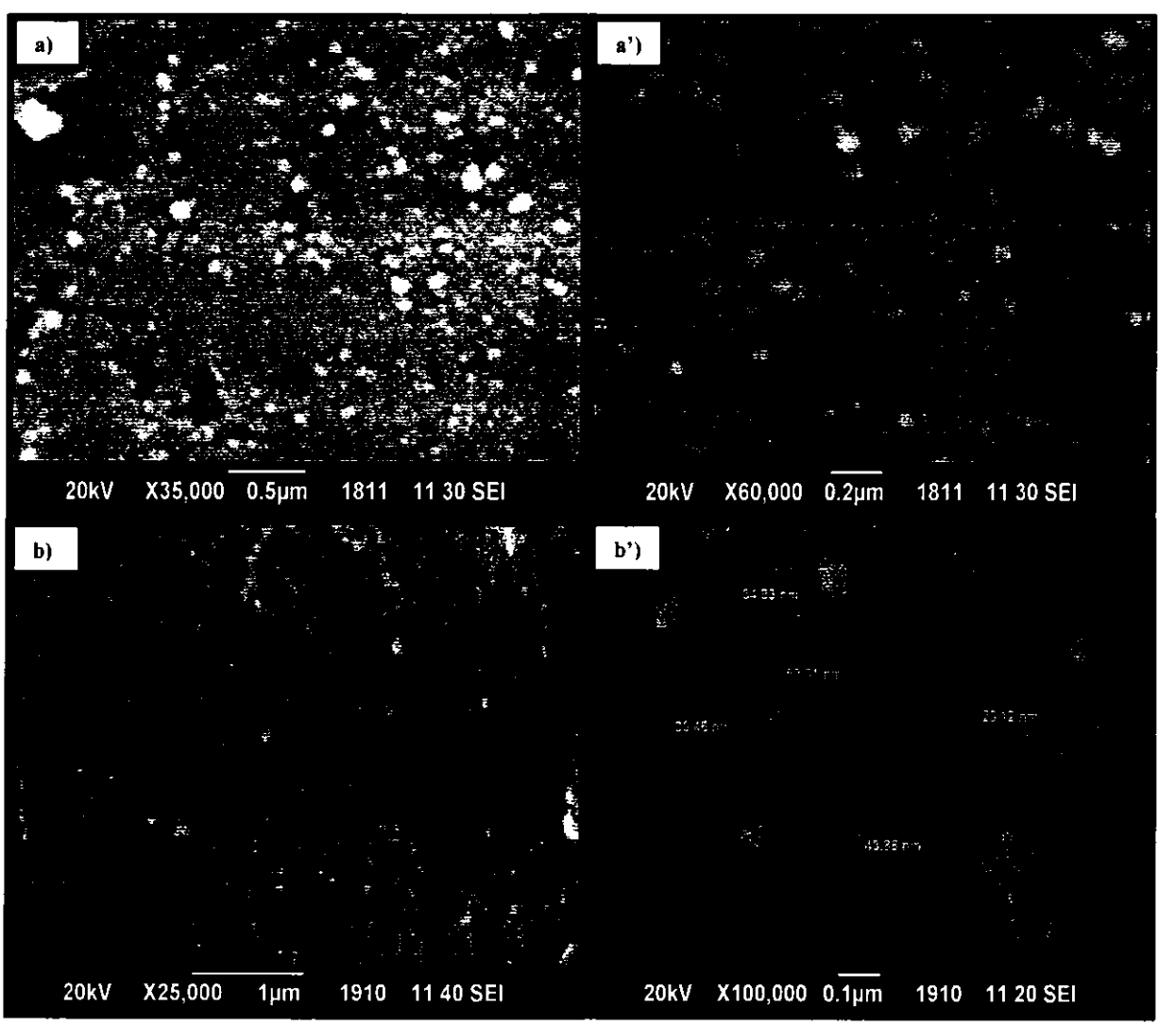

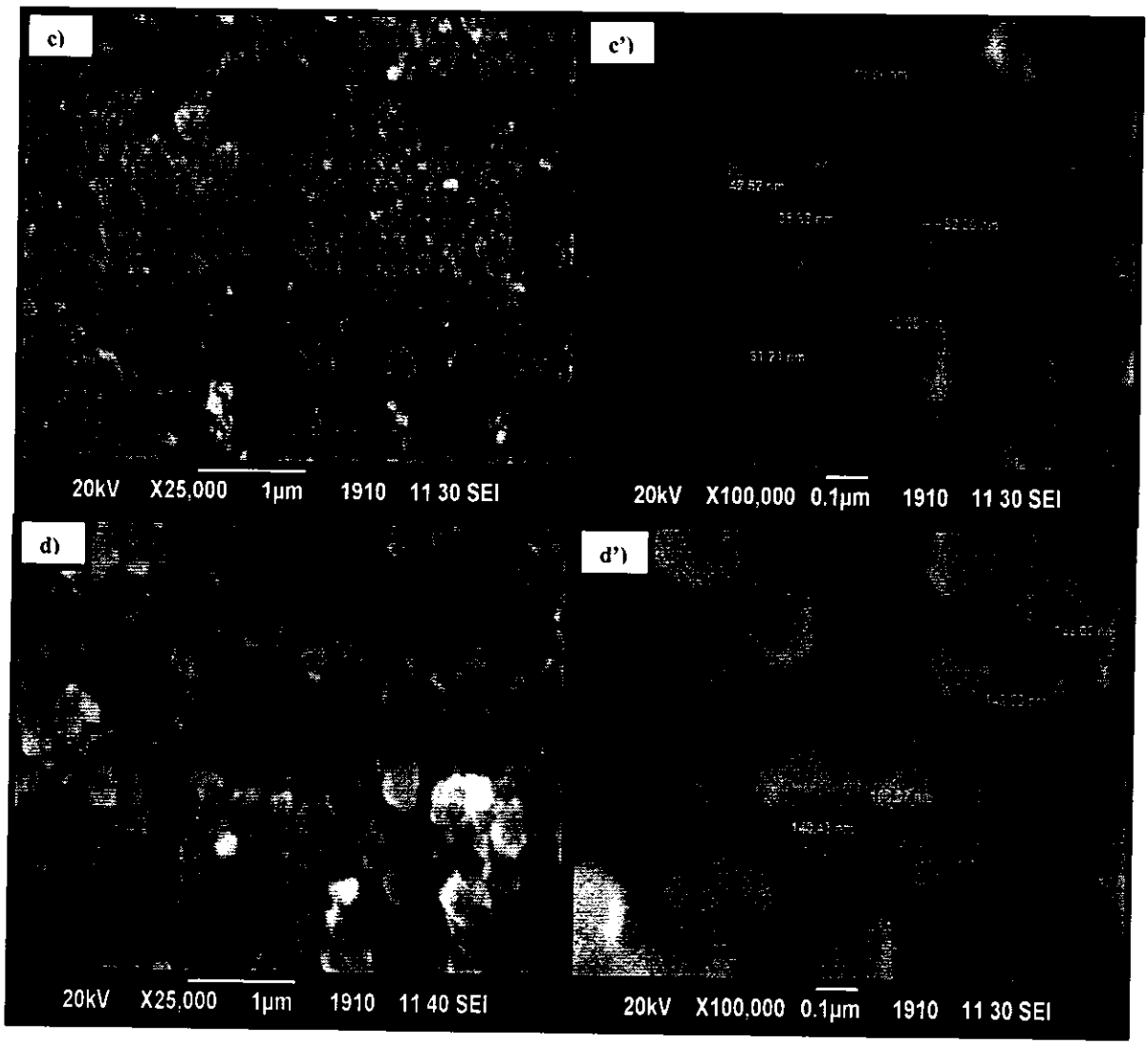

Figure 4.4: SEM micrographs of prepared and annealed nanoparticles taken at different resolutions: a) and a`) as prepared, b) and b`) at 500°C, c) and c`) at 650°C, and d) and d`) at 1000°C.

Table 2: Summary of Annealing Effects on Crystallite Size (D_{xrd}), Lattice Parameter (A), Volume (V), Measured Density (ρ_m), X-Ray Density (ρ_x), Porosity (P), Grain Size, Coercivity (H_c), Saturation Magnetization (M_s), Remanence (M_r) and Energy Band Gap (E_g) of Synthesized Cobalt Zinc Ferrite Nanoparticles.

Parameters	**As prepared**	**500°C**	**650°C**	**1000°C**
D_{XRD} (Å)	245	360	417	416
a(Å)	8.17	8.37	8.39	8.41
V(Å^3)	545.3	586.4	590.6	594.8
ρ_m(gcm^{-3})	4.46	4.10	4.00	3.97
ρ_x (gcm^{-3})	3.87	3.78	3.76	3.75
P (fraction)	0.12	0.08	0.06	0.05
Grain Size(nm)	21	38	44	130
H_c(Oe)	96.88	91.13	135.36	113.58
M_s(emu/g)	19.32	43.37	53.99	66.58
M_r(emu/g)	4.14	9.10	15.16	19.08
M_r/M_s (S/R)	0.21	0.20	0.28	0.29
E_g(eV)	1.71	1.69	1.66	1.59

4.4 Chemical Study

4.4.1 Energy-Dispersive X-ray Spectroscopy (EDX)

Compositional investigations of prepared $Co_{1-x}Zn_xFe_2O_4$ (x = 0.5) nanoparticles acquired by coprecipitation route have been performed through EDX. The chemical composition and contents of the chemicals have been analyzed by EDX spectrums. The chemical peaks of each element for prepared spinel $Co_{1-x}Zn_xFe_2O_4$ (x = 0.5) nanoparticles have been shown in Figure 4.5 and contents in Table 3. The contents of each element has been calculated theoretically and compared with experimental results, and hence, found almost same. Oxygen has been considered as balanced in both cases due to its varying values. In micrographs of EDX, one extra peak appears around 2KeV, which belongs to gold peak. This peak corresponds to gold coating of prepared ferrites, which is requirement of instrument.

Table 3: Compositional Analysis of Ferrite Nanoparticles

Temperature	Experimentally Analysis				Theoretically Calculated			Formulization
Degree	**Co**	**Zn**	**Fe**	**O**	**Co**	**Zn**	**Fe**	$Co_{0.5}Zn_{0.5}Fe_2O_4$
As Prepared	**15.84**	**18.94**	**65.22**	**BALANCED**	**0.45**	**0.50**	**2**	$Co_{0.45}Zn_{0.50}Fe_2O_4$
500	**18.76**	**18.55**	**62.69**		**0.56**	**0.50**	**2**	$Co_{0.56}Zn_{0.50}Fe_2O_4$
650	**17.87**	**19.31**	**62.82**		**0.53**	**0.52**	**2**	$Co_{0.53}Zn_{0.52}Fe_2O_4$
1000	**16.65**	**18.85**	**64.47**		**0.49**	**0.50**	**2**	$Co_{0.49}Zn_{0.50}Fe_2O_4$

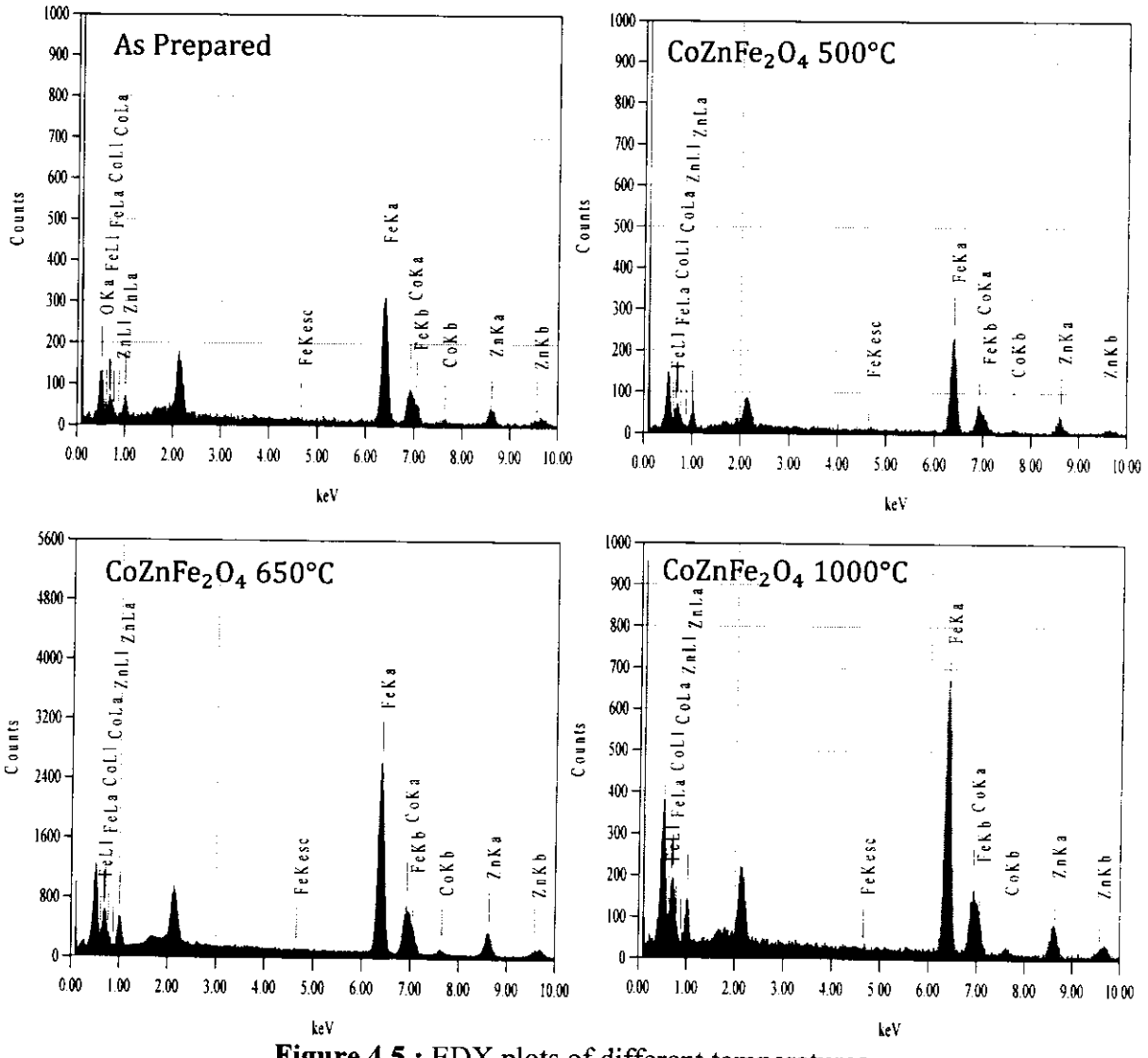

Figure 4.5 : EDX plots of different temperatures.

4.4.2 X-Ray Florescence (XRF)

The compositional analysis of prepared $Co_{1-x}Zn_xFe_2O_4$ (x = 0.5) nanoparticles has been also performed using XRF. It has been confirmed from the XRF micro-plots, that the prepared $Co_{1-x}Zn_xFe_2O_4$ (x = 0.5) spinel ferrite nanoparticles are composed of Cobalt, Zinc and Iron in specific ratio of 0.5:0.5:1, respectively. Figure 4.6 shows and verifies the presence contents of each synthesized $Co_{1-x}Zn_xFe_2O_4$ (x = 0.5) spinel ferrite samples annealed at 500°C, 650°C and 1000°C temperatures.

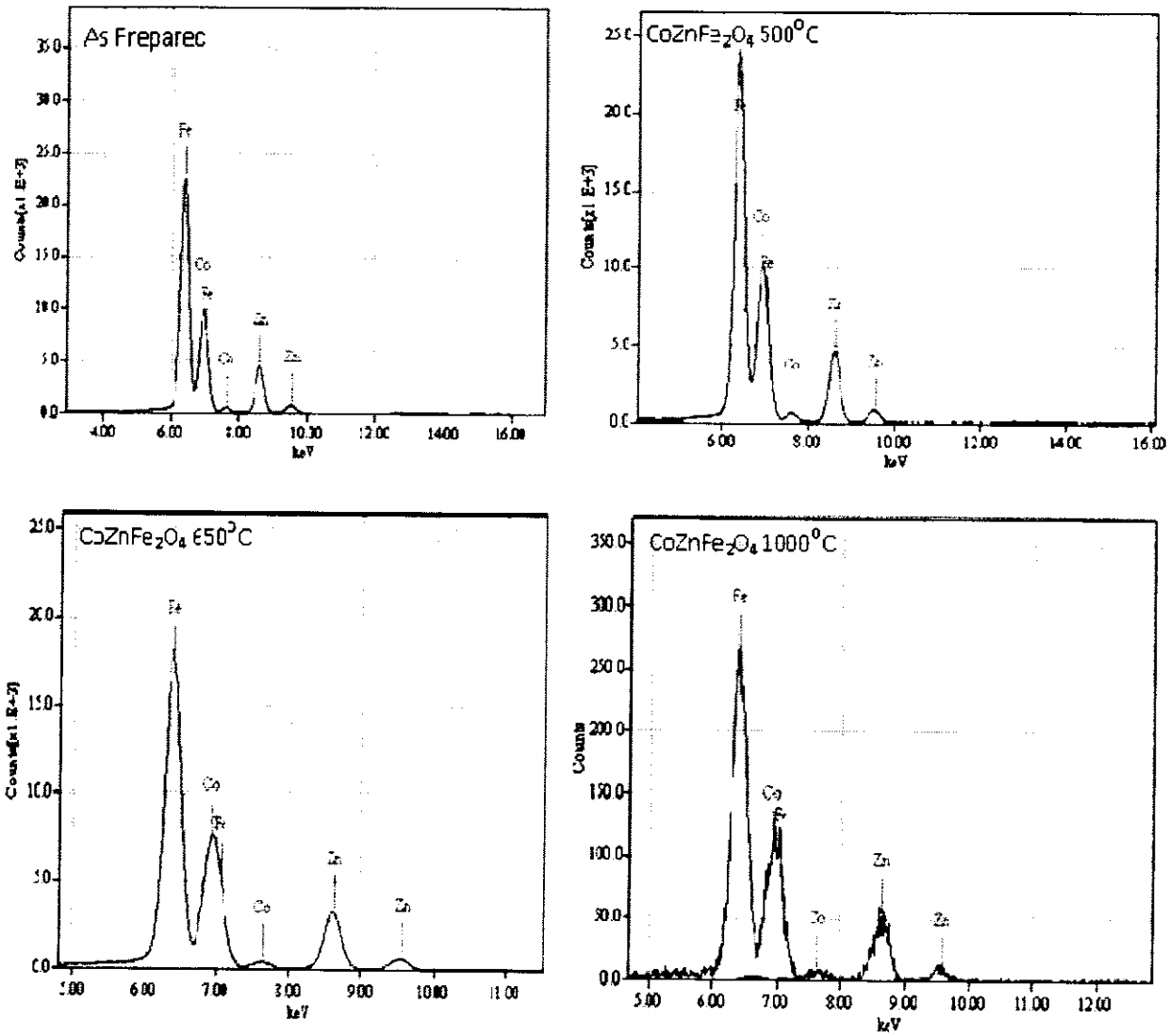

Figure 4.6: XRF study of nanoparticles.

4.5 Magnetic Characterization

The magnetic measurements of prepared and annealed $Co_{1-x}Zn_xFe_2O_4$ (x = 0.5) nanoparticles have been carried out at room temperature using vibrating sample magnetometer (VSM). The variation of magnetization as function of applied field at room temperature for $Co_{1-x}Zn_xFe_2O_4$ (x = 0.5) nanoparticles annealed at 500°C, 650°C and 1000°C temperatures has been shown in Figure 4.7. These M-H curve loops have been measured by applying an external magnetic field of 8000 Oe. All the samples exhibit very clear M-H loops.

The contracted loops of VSM identify soft nature of $Co_{1-x}Zn_xFe_2O_4$ (x = 0.5) nanoparticles. The behavior of all the curves appears normal but the magnetization increases with increasing applied field as shown in Figure 4.8. It has been observed that the magnetic properties of prepared $Co_{1-x}Zn_xFe_2O_4$ (x = 0.5) nanoparticles are highly influenced through annealing process. Magnetic characteristics like saturation magnetization, coercivity and remanence depends on annealing temperature and these parameters have been estimated from hysteresis curves and tabulated in Table 2.

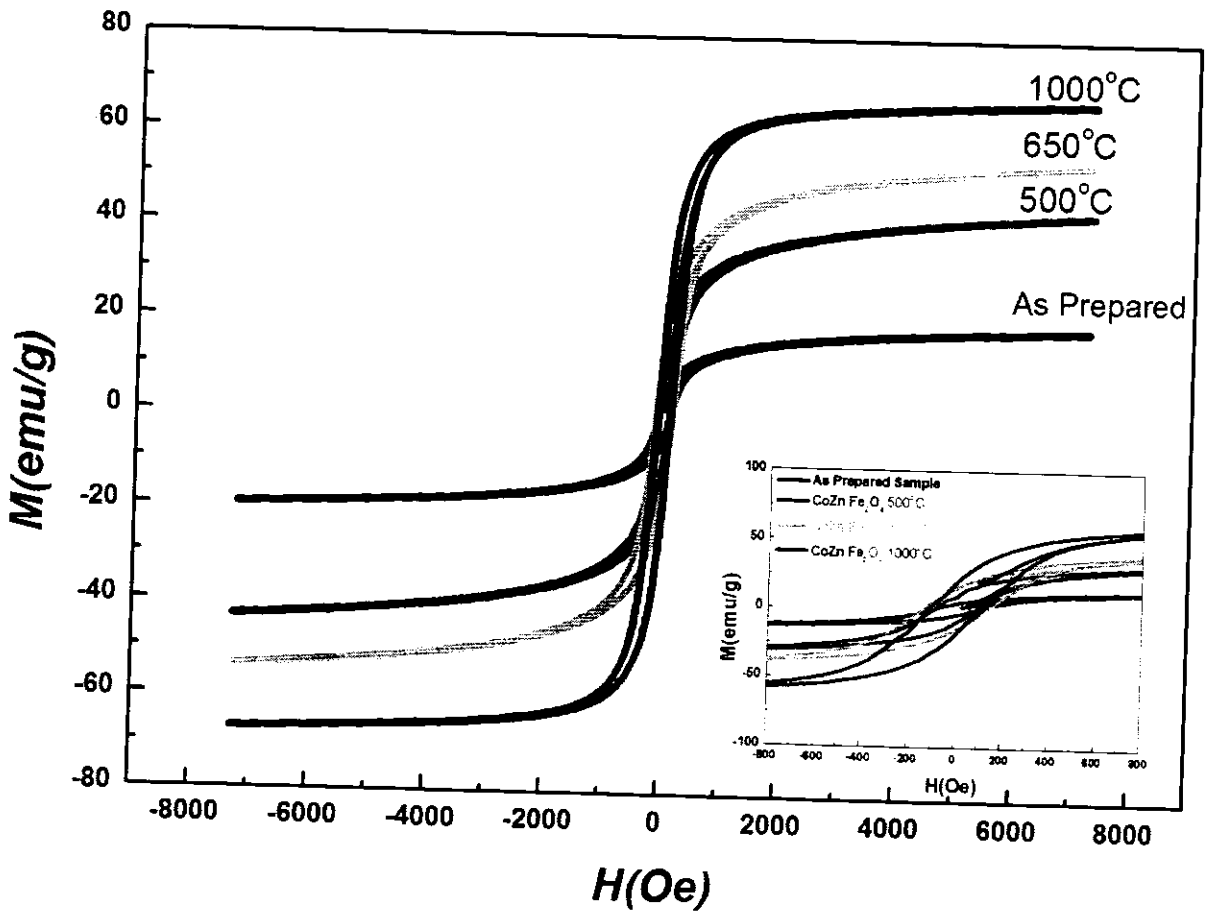

Figure 4.7: M-H loops of CoZn ferrite nanoparticles.

The behaviour of coercivity as a function of annealing temperature of prepared $Co_{1-x}Zn_xFe_2O_4$ (x = 0.5) nanoparticles is shown in Figure 4.8 and presented in Table 2. Surface anisotropy, magneto-crystalline anisotropy and antiparticle interactions, crystal anisotropy and critical diameter are some anisotropy mechanisms that govern the magnetic properties of ferrite nanoparticles [7]. The magnetic field strength has been represented by coercivity which is essential

to anticipate the anisotropy barrier and permit magnetization. In ferrimagnetic spinels, the superexchange interactions influence magnetic ordering of ferrites that actually occurs between A and B sublattice metal ions. These exchange interactions are reduced by substitution of nonmagnetic ions at A and B sites. According to Neel's two sublattice model of ferrimagnetism, the net magnetic moments of A and B sublattice per formula unit $n_B^N(x)$ can be elaborated as [41]:

$$n_B^N(x) = M_B(x) - M_A(x) \qquad (4.5)$$

Where M_B represents B sublattice moment and M_A as A sublattice moments. The behaviour of coercivity H_c has been highly influenced by the temperature of the prepared samples. It has been seen from previous studies that coercivity tends to vanish with increase in temperature in superparamagnetic specimen [71].

Inset of Figure 4.7 shows the anisotropy of the prepared $Co_{1-x}Zn_xFe_2O_4$ (x = 0.5) nanoparticles. Figure 4.8 shows sinusoidal behavior of coercive field for as prepared $Co_{1-x}Zn_xFe_2O_4$ (x = 0.5) nanoparticles. The H_c got significant values ranging between 135.8 Oe – 91.88 Oe for various annealing temperatures of $Co_{1-x}Zn_xFe_2O_4$ (x = 0.5) nanoparticles as shown in Figure 4.8.

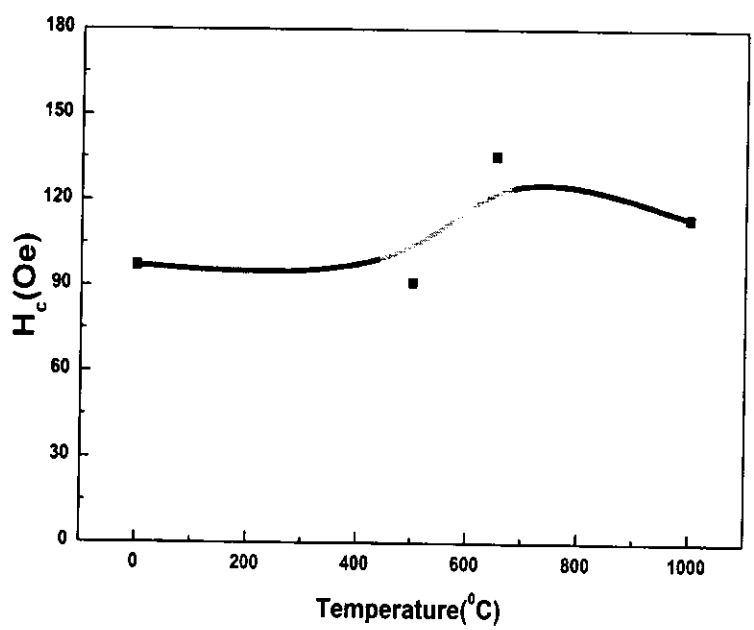

Figure 4.8: Coercivity as function of annealing temperature.

When applied field is removed, the samples give zero net magnetic moment when their spins are relaxed back by rotation. The saddle points reflect variation in H_c with increasing values of annealing temperature of nanoparticles as shown in Figure 4.8. The variations of H_c with grain size could be explained on the basis of domain structure and anisotropy of crystal [7]. The H_c first decreases from 96.88 Oe to 91.88 Oe due to multi-domain region as the particle diameter increases. Then at 650°C, H_c increases up to 135.8 Oe. Upon further annealing, the value of H_c again decreases due to increase in crystallite size. The value of H_c reaches maximum value and then decreases as the grain size increases. By the increase in crystallite size, the number of grain boundaries increases and consequently H_c of nanoparticles decrease. Hence, the decrease in H_c with increasing value of annealing temperature attributes to decrease in anisotropy field that in response decreases domain wall energy.

The saturation magnetization M_s and remanence M_r have been calculated from M-H loops and results of their values are given in Table 2. Both the M_s and M_r increases with increasing annealing temperature of prepared nanoparticles. The trend for M_s shows that M_s increases from 19.32 $emug^{-1}$ to 66.58 $emug^{-1}$ as shown in Figure 4.9. The M_r trend also shows increasing values of M_r from 4.41 $emug^{-1}$ to 19.08 $emug^{-1}$ with increasing annealing temperature of

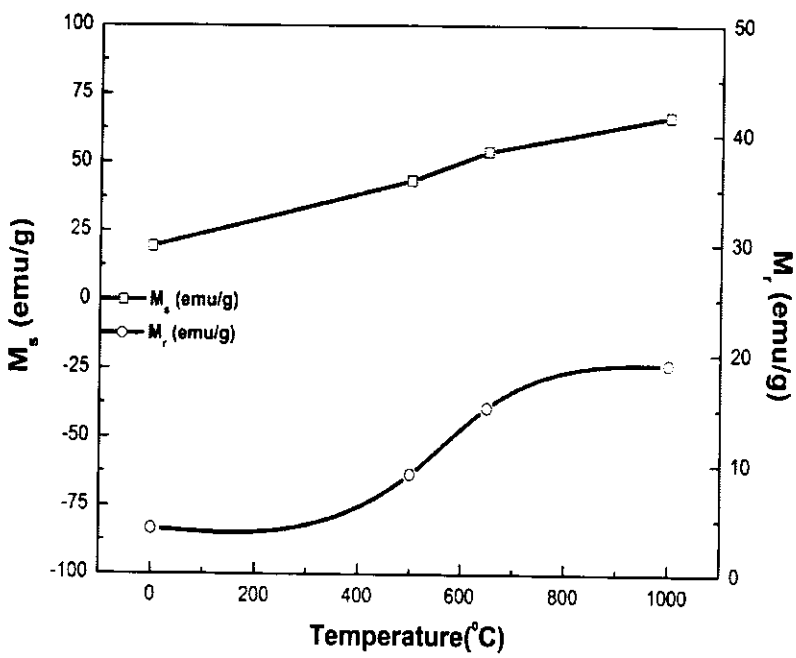

Figure 4.9: Plot of M_s and M_r Verses annealing temperature.

$Co_{1-x}Zn_xFe_2O_4$ (x = 0.5) nanoparticles. The increasing fashion of M_s and M_r with increasing values of annealing temperature of $Co_{1-x}Zn_xFe_2O_4$ (x = 0.5) nanoparticles can be explicated by Neel's theory [72]. Both M_s and M_r increases because Zn^{2+} with zero magnetic moment replicate tetrahedral A-site ions which compel to decrease moment in sublattice M_A by increasing net magnetic moment. The increasing values of M_s and M_r also significantly influenced by variation in annealing temperature due to steady increase in particle size and crystallinity. The results obtained by VSM are in good agreement with previously reported behaviors of magnetic materials [65, 73].

In order to further explore the magnetic properties of as prepared and annealed nanoparticles, the M_r / M_s is plotted as function of annealing temperature and their behavior is shown in Figure 4.10. The trend of M_r / M_s of synthesized $Co_{1-x}Zn_xFe_2O_4$ (x = 0.5) nanoparticles indicates that at room temperature considerable amount of nanoparticles are still superparamagnetic in the absence of externally applied magnetic field.

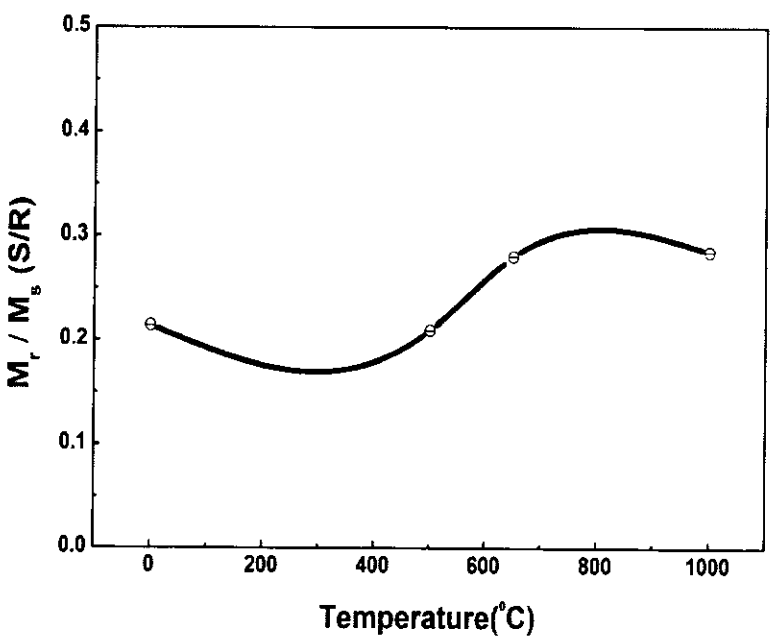

Figure 4.10: Plot of ratio of M_s and M_r Verses annealing temperature.

Thus, by variation in annealing temperature of magnetic nanoparticles; the magnetic properties of the prepared $Co_{1-x}Zn_xFe_2O_4$ (x = 0.5) nanoparticles have been changed. Hence,

annealing causes changes by the transformation or decomposition of phases which brings increase in grain size, pore size number and shape.

4.6 Optical Study

4.6.1 Diffuse Reflectance

To measure the optical properties, versatile Lambda 950 double beam spectrometer has been used, operating in the UV spectral ranges. The diffuse reflectance spectra of various prepared $Co_{1-x}Zn_xFe_2O_4$ (x = 0.5) nanoparticles annealed at 500°C, 650°C and 1000°C temperatures is shown in Figure 4.11.

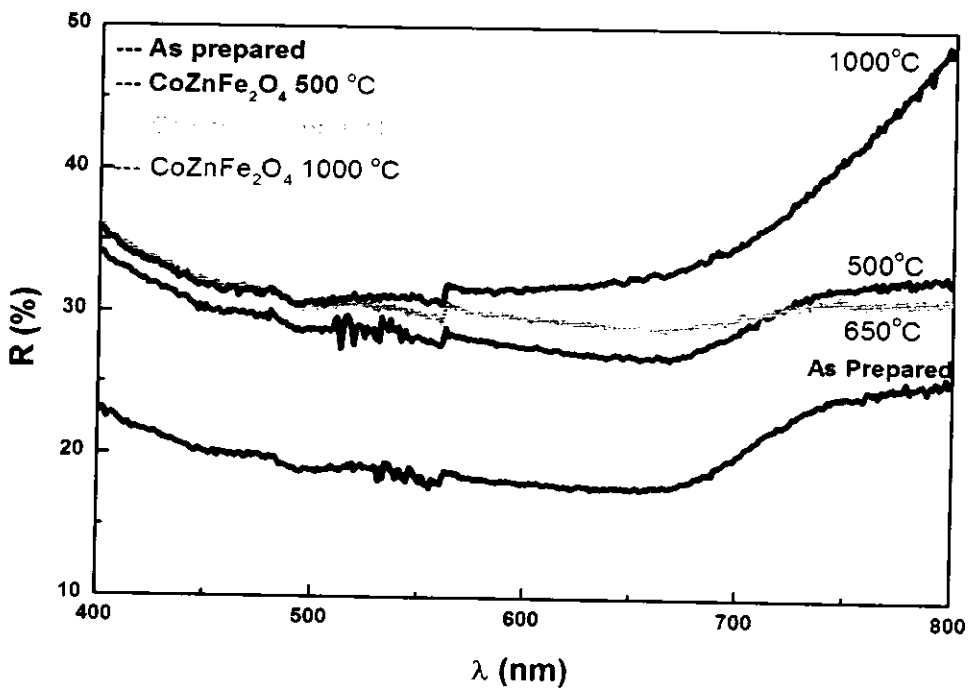

Figure 4.11: Diffuse reflectance spectra of annealed $Co_{1-x}Zn_xFe_2O_4$ (x = 0.5) nanoparticles.

Figure 4.11, it is obvious that $Co_{1-x}Zn_xFe_2O_4$ (x = 0.5) nanoparticles exhibit highest values of percentage diffuse reflectance with increasing values of annealing temperature. The sudden variation at a specific wavelength reflects the presence of optical band gap in prepared $Co_{1-x}Zn_xFe_2O_4$ (x = 0.5) nanoparticles. Moreover, the diffuse reflectance percentage of all the prepared $Co_{1-x}Zn_xFe_2O_4$ (x = 0.5) nanoparticles increases with the increase in annealing temperature (0°C - 1000°C) from 26.6 % to 48.9 %. The as prepared $Co_{1-x}Zn_xFe_2O_4$ (x = 0.5)

nanoparticles show significant increase in diffuse reflectance as compared to previously reported Cobalt ferrites [74]. The increase in percentage diffuse reflectance has been due to colorations effect on the optical properties of the ferrites by doping of Zinc (Zn^{2+}) ions which substitute Cobalt (Co^{2+}) ions in $Co_{1-x}Zn_xFe_2O_4$ (x = 0.5) structures. When incident beam light falls on surface of prepared $Co_{1-x}Zn_xFe_2O_4$ (x = 0.5) nanoparticles then a fraction of beam is reflected whereas the rest is penetrated into mass. This penetrated beam endure scattering via diffraction, refraction and manifold reflection, in addition to absorption inside colored material that is highly dependent on material. During the motion of diffused rays within the material, they loss several wavelengths and will emerge colored. Among few of the radiations eventually leave mass in all directions which results in diffused reflectance light [74].

4.6.2 Band Gap

The energy band gap 'E_g' has been determined from reflectance spectra of synthesized $Co_{1-x}Zn_xFe_2O_4$ (x = 0.5) nanoparticles within wavelength range of 400nm - 800nm at room temperature. In general, the E_g of the samples can be estimated in two ways; (i) from reflectance spectra and (ii) using standard relations. The energy gap of prepared $Co_{1-x}Zn_xFe_2O_4$ (x = 0.5) nanoparticles can be calculated from the reflectance spectra using following relation:

$$E_g = \frac{1240eV}{\lambda} \qquad (4.6)$$

Where "λ" is the wavelength at which diffused reflectance spectra has been obtained. The absorption coefficient "α" can be calculated by using relation 4.7;

$$\alpha = \frac{(1-R)^2}{2R} \qquad (4.7)$$

Where "R" is percentage reflectance of the prepared $Co_{1-x}Zn_xFe_2O_4$ (x = 0.5) samples. For direct band gap materials, absorption coefficient "α^2" has been used. The graph between energy in eV (along abscissa) and absorption coefficient α^2 of prepared and annealed $Co_{1-x}Zn_xFe_2O_4$ (x = 0.5) nanoparticles has been plotted and shown in Figure 4.12. The energy band gap can be obtained by extrapolation of linear part of spectra towards x-intercept.

It is cleared from Figures 4.12-4.13 and Table 2 that E_g has been decreased with increasing the annealing temperature of the synthesized $Co_{1-x}Zn_xFe_2O_4$ (x = 0.5) nanoparticles. Figure 4.12 indicates that the values of E_g of each sample comes out to be 1.71eV, 1.69eV, 1.66eV and 1.59eV for 500°C, 650°C and 1000°C annealing temperature respectively. The decrease in E_g has been due to increase in lattice parameter with increasing values of annealing temperature of $Co_{1-x}Zn_xFe_2O_4$ (x = 0.5) nanoparticles.

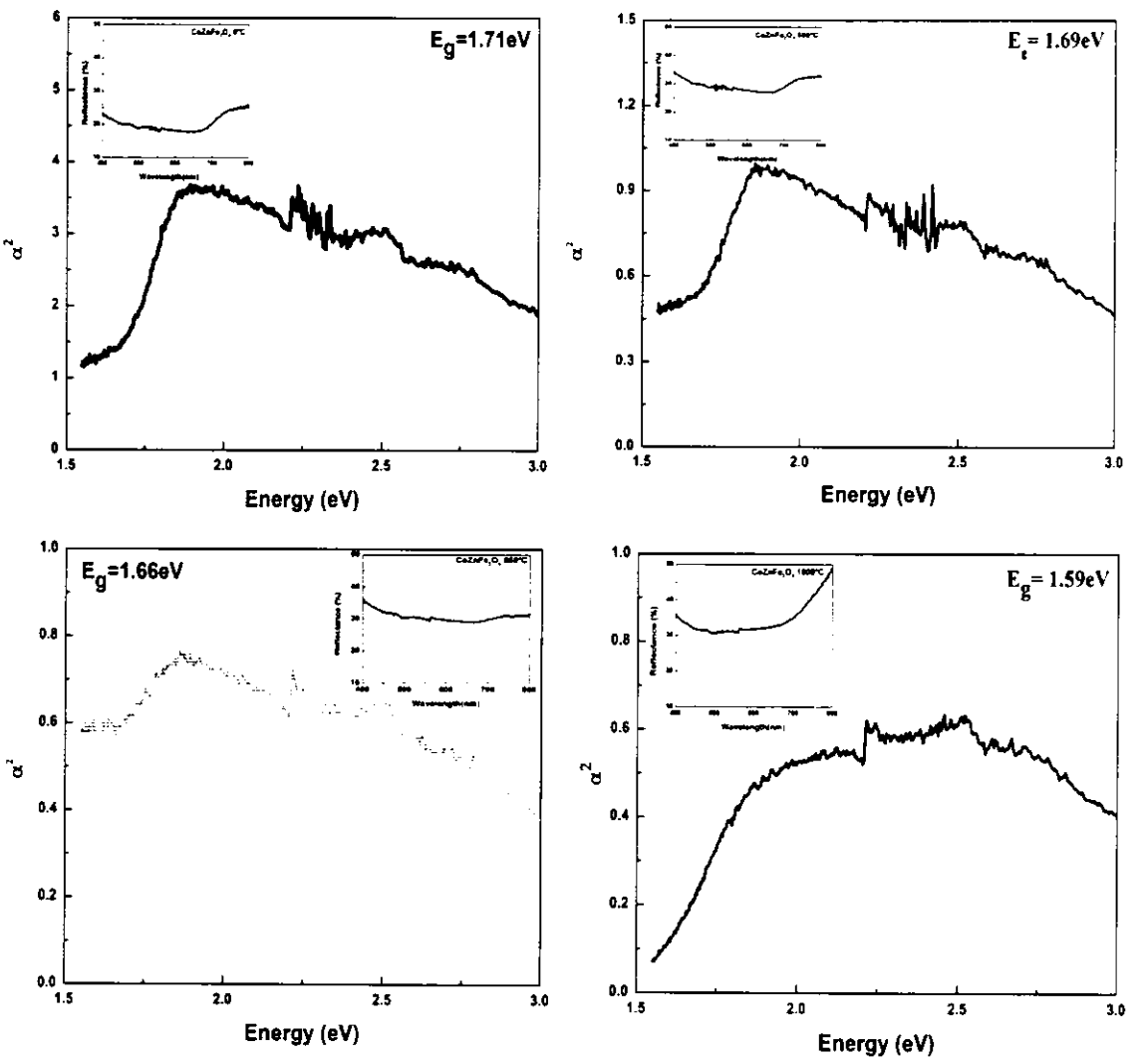

Figure 4.12: Calculation of band gap for various (a) As Prepared, (b) 500°C, (c) 650°C, (d) 1000°C annealing temperature.

Figure 4.13 shows that the E_g decreases as the lattice parameter of prepared samples increases with increase in annealing due to quantum confinement. Therefore, we can conclude on

the basis of increase in lattice parameter, the E_g decreases by increase in annealing temperature of $Co_{1-x}Zn_xFe_2O_4$ (x = 0.5) nanoparticles (Figure 4.12- 4.13).

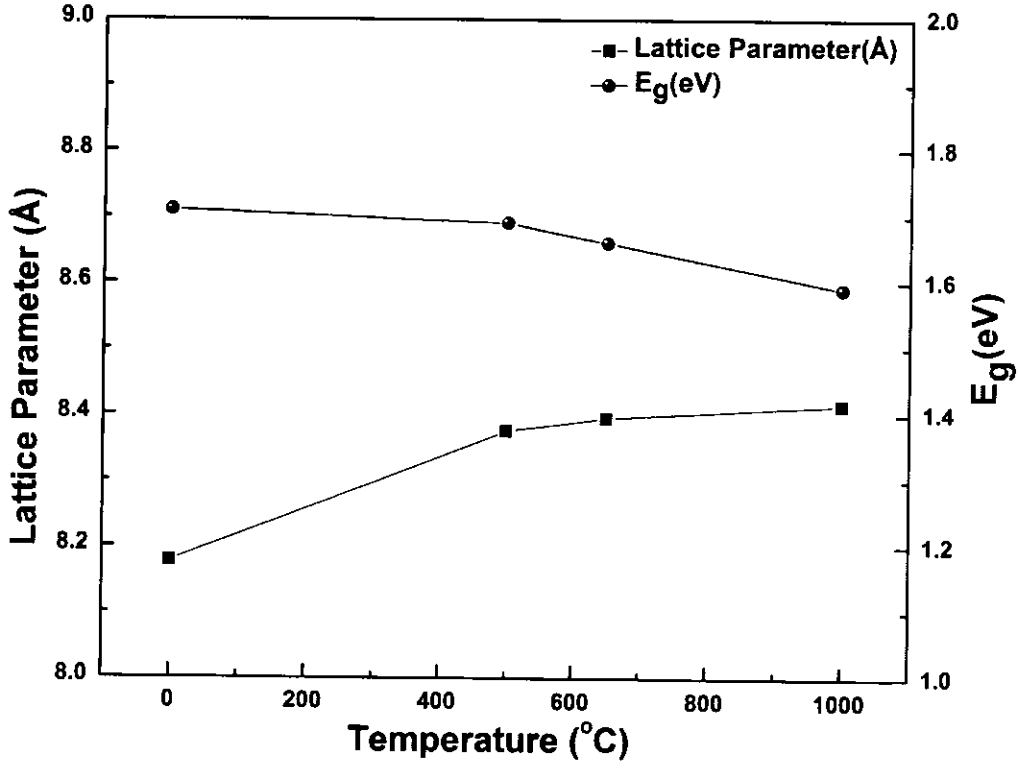

Figure 4.13: Variation of band gap and lattice parameter vs. annealing temperature.

Conclusions

The spinel $Co_{1-x}Zn_xFe_2O_4$ (x = 0.5) nanoparticles have been successfully synthesized by easy, low temperature, high purity and less time consumption chemical coprecipitation route. The different synthesis parameters which are found to be significant have been optimized in order to get controlled size nanoparticles.

The prepared and annealed $Co_{1-x}Zn_xFe_2O_4$ (x = 0.5) nanoparticles have single phase crystallinity with clear diffraction patterns. It has been observed that the width of diffraction peaks contracts as the annealing temperature increases due to increase in grain size of ferrite nanoparticles. The lattice parameter has been found increasing with increase in annealing temperature. This is just because of large ionic radii of Zinc in contrast with Cobalt. The size of particle has been found between 21 nm – 130 nm for prepared $Co_{0.5}Zn_{0.5}Fe_2O_4$ nanoparticles.

EDX and XRF micro-plots confirmed that the prepared $Co_{1-x}Zn_xFe_2O_4$ (x = 0.5) spinel nanoparticles have been composed of Cobalt, Zinc and Iron in specific ratio.

The magnetic moment is found to be improved significantly due to annealing of prepared $Co_{1-x}Zn_xFe_2O_4$ (x = 0.5) nanoparticles. The coercivity shows sinusoidal behavior and got significant values. The saddle points reflect variation in H_c with increasing values of annealing temperature of nanoparticles. The H_c first decreases due to multi-domain region as the particle diameter increases. Then at 650°C, the coercive force increases and upon further annealing, the value of H_c decreases due to increase in crystallite size. By the increase in crystallite size, the number of grain boundaries decreases and consequently H_c of nanoparticles decrease. The saturation magnetization M_s and remanence M_r have been found to be increasing because of Zn^{2+} with zero magnetic moment replicate tetrahedral A-site ions which compel to decrease moment in sublattice M_A by increasing net magnetic moment. The increasing values of M_s and M_r also significantly influenced by variation in annealing temperature due to steady increase in particle size and crystallinity. The behavior of M_r / M_s indicates that at room temperature considerable amount of nanoparticles are still superparamagnetic in the absence of externally applied magnetic field.

CONCLUSIONS

$Co_{1-x}Zn_xFe_2O_4$ (x = 0.5) nanoparticles exhibit highest values of percentage diffuse reflectance with increasing values of annealing temperature. The optical properties have shown tailoring in band gap as function of annealing temperature. The optical energy band gap of prepared nanoparticles has been found to be decreasing. The decrease in E_g can be due to increase in lattice parameter with increasing values of annealing temperature because of quantum confinement.

Hence, we can conclude that annealing of $Co_{0.5}Zn_{0.5}Fe_2O_4$ nanoparticles induces effects on physical characteristics by the transformation or decomposition of phases which brings increase in grain size, pore size number and shape.

References

[1] Sergry P. Gubin, (2009) Magnetic Nanoparticles. Taylor and Fransic. A, p 89.

[2] I. Safarik, M. Safarikova, (2002) Magnetic Nanoparticles and Bioscience, Monotshefte fut Cemie, 133,737.

[3] T. Vo- Dihn, B. Cullum, D. Stokes, (2001) Nanosensors and Biochips, Frontiers in Bimolecular Diagnostics, Sensors and Actuators B, 2, p. 74.

[4] P. Weiss, (1907) J.Phys. 6,401.

[5] A. Goldman, (1990) Modern Ferrite Technology. New York, Van Nostrand Reinhold.

[6] N. Spaldin, (2003) Magnetic materials, Fundamentals and Device Applications. Cambridge: Cambridge University press.

[7] B. D. Cullity, (1972) Introduction to Magnetic Materials, p. 248,284.

[8] A. K. Bandyopadhyay, (2008) Nanomaterials, p. 171-173, 174-175, 177.

[9] David Jiles, (2008-09) Introduction to Magnetism and Magnetic Materials, Second Edition, Taylor and Fransic, p 89.

[10] P. Auric, J. Chappert, A. K. Bandyopadhyay, J. Zarzycki, (1982) Superparamagnetism And Ferrimagnetism of The Small Particles of Magnetite in A Silicate Matrix, J. Non-Crystalline Solids, 50, 97.

[11] L. Neel, (1949) C. R. Acad. Sci., 229, 664.

[12] R. E. Rosensweig, (1958) Ferrohydrodynamics Mineola, New York, Dover Publications, INC.

[13] K. Raj, B. Moskowitz, R. Casciari, (1995) Advances in Ferrofluids Technology, Journal of Magnetism and Magnetic Materials, 149, 174.

[14] G. F. M. Pires, A. S. B. Sombra, M. M. Costa, Dielectrics and Impedance Properties.

[15] J. Smit, H. P. J. Wijn, (1959) Ferrites, Jhon Wiley and Sons, New York.

[16] A. Goldman, (1999) Handbook of Modern Ferromagnetic Materials, The Springer International Series in Engineering and Computer Science, Springer, New York.

[17] J. A. Paulsen, A. P. Ring, C. C. H. Lo, J. E. Snyderb, D.C. Jiles, (2005) Manganese-Substituted Cobalt Ferrite Magnetostrictive Materials For Magnetic Stress Sensor Applications, J. Appl. Phys. 97, p. 04502–04505.

[18] Maziewski et al., (1977) Visual Observation of Phase Domains in Dysprosium Orthoferrite, J. Phys. D: Appl. Phys. 10, p. L37-L38.

[19] K. J. Standley, (1972) Oxide Magnetic Materials, 2nd ed., Oxford University Press.

[20] V. Blaskov, V. Petkov, V. Rusanov, L. M. Martinez, B. Martinez, J. S. Munoz, M. Mikhov, (1996) J. Magn. Magn. Mater. 162, p. 331–335.

[21] S. Chickazumi, S. H. Charap, (1978) Physics of Magnetism, Krieger Malabar.

[22] R. K. Puri, V. K. Babbar, (1997) Solid State Physics and Electronics, S. Chand and Company LTD.

[23] David Jiles, (1998) Introduction to Magnetism and Magnetic Materials, First Edition, p. 349.

[24] M. S. Vijaya, G. Rangarajan, (1999-2000) Materials Science, McGraw-Hill Publishing Company Limited, New Delhi, p. 447.

[25] Robert W. Cahn, R. W. Cahn, Peter Haasen, (1996) Physical Metallurgy, 4th Edition, 1, p. 2522.

[26] V. G. Bashtovoy, B. M. Berkovsky, A. N. Vislovich, (1998) Introduction to Magnetic Fluids, Washington.

[27] T. Albrecht, C. Bührer et al., (1997) Appl. Phys. A. Materials Science and Processing, 65, 215A.

[28] R. Valenzuela, (1984) Magnetic Ceramics, Cambridge University Press, Cambridge, p. 191-212.

[29] K. Raj, R. Moskowitz, R. Casciari, (1995) Advances in Ferrofluids Technology, J. Magn. Magn. Mater, 149, p. 174-180.

[30] M. U. Islam, M. U. Rana, T. Abbbas, (1998) Study of Magnetic Interactions in Co-Zn-Fe-O System, Materials Chemistry and Physics, 57, p. 190- 193.

[31] Tawfik, I. M. Hamada, O. M. Hemeda, (2002) Effect of Laser Irradiation on the Structure and Electromechanical Properties of Co-Zn Ferrite, J. Magn. Mater, 250, p. 77-82.

[32] Dey, J. Ghose, (2003) Synthesis, Characterization and Magnetic Studies on Nanocrystalline $Co_{0.2}Zn_{0.8}Fe_2O_4$, Materials Research Bulletin, 38, p. 1653-1660.

[33] R. Arulmurugan, B. Jeyadevan, G. Vaidyanathan, S. Sendhilnathan, (2005) Effect of Zinc Substitution on Co-Zn and Mn-Zn Ferrite Nanoparticles Prepared by Co-Precipitation, J. Magn. Mater. 288, p. 470-477.

[34] Ana Maria Rangel de Figueiredo Teixeiraa, Tsuneharu Ogasawarab, Maria Cecília de Souza Nóbrega, (2006) Investigation of Sintered Cobalt-Zinc Ferrite Synthesized by

Coprecipitation at Different Temperatures: A Relation between Microstructure and Hysteresis Curves, Materials Research, 9, p. 257-262.

[35] D. S. Mathew, R.S. Juang, (2007) J. of Chem. Eng., 129, p. 51-65.

[36] M. J. Iqbal, M. R. Siddiquah, (2008) Electrical and Magnetic Properties of Chromium Substituted Cobalt Ferrite Nanomaterials, J Alloy Compd, 453, p. 1-9.

[37] WS Chiu, S. Radiman, R. Abd-Shukor, M. H. Abdullah, P. S. Khiew, (2008) Tunable Coercivity of $CoFe_2O_4$ Nanoparticles Via Thermal Annealing Treatment, J Alloy Compd, 459, p. 291-297.

[38] Y. Koseog˘lu, A. Baykal, F. Gozuak, H. Kavas, (2009) Structural and Magnetic Properties of $Co_xZn_{1-x}Fe_2O_4$ Nanocrystals Synthesized By Microwave Method, Polyhedron 28, p. 2887–2892.

[39] S. B. Waje, M. Hashim, W. D. W. Yousoff, Z. Abbas, (2010) Sintering Temperature Dependence of Room Temperature Magnetic and Dielectric Properties of $Co_{0.5}Zn_{0.5}$ Fe_2O_4 Prepared Using Mechanically Alloyed Nanoparticles, J. Magn. Mater., 322, p. 686-691.

[40] M. H. Yousefi, S. Manouchehri, A. Arab, M. Mozaffari, Gh. R. Amiri, J. Amighian, (2010) Materials Research Bulletin 45, p. 1792–1795.

[41] Sonal Singhal, Tsering Namgyal, Sandeep Bansal, Kailash Chandra, (2010) Effect of Zn Substitution on the Magnetic Properties of Cobalt Ferrite Nano Particles Prepared Via Sol-Gel Route, J. Electromagnetic Analysis & Applications, 2, p. 376-381.

[42] M. Mozaffari, S. Manouchehri, M. H. Yousefi, J. Amighian, (2010) The Effect of Solution Temperature on Crystallite Size and Magnetic Properties of Zn Substituted Co Ferrite Nanoparticles, J. Magn. Mater., 322, p. 383–388.

[43] X. Q. Shen, J. Xiang, F. Z. Song, M. Q. Liu, (2010) Appl Phys, 99, p. 189–195.

[44] A. R. Jelvani, Gh. R. Amiri, S. Fatahian, S. Manouchehria, M. Habibi, R. Mousarezaei Dehaghi, (2011) Optoelectronics and Advanced Materials, 5, p. 1216-1218.

[45] Harshida Parmar, Rucha Desai, R. V. Upadhyay, (2011) Structural Characterization of Microwave-Synthesized Zinc-Substituted Cobalt Ferrite Nanoparticles, Appl. Phys. A, 104, p. 229–234.

[46] J. Lopez, L. F. Gonzalez- Bahamon, J. Prado , J. C. Caicedo, G. Zambrano, M. E. Gomez, J. Esteve, P. Prieto, (2012) Study of Magnetic and Structural Properties of Ferrofluids Based on Cobalt–Zinc Ferrite Nanoparticles, J. Magn. Magn. Mater., 324, p. 394–402.

[47] A. Hassadee, T. Jutarosaga, W. Onreabroy, (2012) Effect of Zinc Substitution on Structural and Magnetic Properties of Cobalt Ferrite, Procedia Engineering, 32, p. 597-602.

[48] Ritu Rani , S. K. Sharma, K. R. Pirota, M. Knobel, Sangeeta Thakur, M. Singh, (2012) Effect of Zinc Concentration on the Magnetic Properties of Cobalt–Zinc Nanoferrites, Ceramics International, 38, p. 2389-2394.

[49] H. Y. He: J. Mater Sci., (2012) Mater Electron, 23, p. 995–1000.

[50] B. D. Cullity, (1978) Element of XRD, 2nd Edition, Addision - Wesley, New York.

[51] K. L. Horovitz, V. A. Johnson, (1959) Solid State Physics, 6, Academic Press, New York and London.

[52] J. Smit, H. P. J. Wijn,(1959) Ferrites, Jhon Wiley and Sons, New York.

[53] R. E. Ferrell, G. G. Paulson, (1973) An Ortec Workshop, Energy Dispersive Analysis of X-ray Spectra Generated in the SEM, Braniff Place, New Orleans, Louisian.

[54] A. K. Bandyopadhyay, P. Auric, (1987) Hyperfine Splitting and Anisotropy of Magnetite Particles within a Glass Matrix by Mössbauer Spectroscopy, Trans. Ind. Ceram. Soc., 46, p. 136.

[55] E. Auzans, (1999) Thesis on Mn-Zn Ferrite Nanoparticles Based On the Properties and Preparation of Ferrofluids, IOP, LU, France.

[56] P. C. Kuo, T. S. Tsai, (1989) J. Appl. Phys. 65, p. 4349.

[57] M. Khoudiakov, M. C. Gupta, S. Deevi, (2004) Nanotechnology 15, p. 987.

[58] B. H. Ryu, H. J.Chang, Y. M. Choi, K. J. Kong, J. O. Lee, C. G. Kim, H. K. Jung, J. H. Byun, (2004) Phys. Solid State 201, p. 1855.

[59] A. Faraz, M. Saqib, N. M. Ahmad, F. Rehman, A. Maqsood, M. Usman, A. Mumtaz, M. A. Hassan, (2012) J Supercond. Nov Magn., 25, p. 91-100.

[60] R. K. Sharma, O. Suwalka, N. Lakshmi, K. Venugopalan, A. Banerjee, P. A. Joy, (2005) Mater. Lett., 59, p. 3402.

[61] C. dong, (1999) J. Appl. Crystallogr. 32, p. 838.

[62] A. A. Sattar, H. M. El-Sayed, W. R. Agami, A. A. Ghani, (2007) Am. J. Appl. Sci., 4, p. 89.

[63] R. Parker, H. Lords, (1962) Proc. Phys. Soc. A, 79, p. 383.

[64] X. Q. Shen, J. Xiang, F. Z. Song, M. Q. Liu., (2010) Appl. Phys. A., 99, p. 189-195.

[65] G. Vaidyanthan, S. Sendhilnathan, R. Arulmurugan, (2007) J. Magn. Magn. Mater., 313, p. 293-299.

[66] C. C. Berry, G. Curtis, (2003) J. Phys. D, Appl. Phys., 36, p. R198.

[67] S. S. More, R. H. Kadam, A. B. Kadam, D. R. Mane, G. K. Bichile, (2010) Cent. Eur. J. Chem., 8, p. 419.

[68] S. Nasir, M. Anis-ur Rehman, (2011) Phys. Scr. 84, 025603, p. 7.

[69] B. R. Karche, B. V. Khasbardar, A. S. Vaingankar, (2003) Physica C, Supercond., 387, p. 290.

[70] A. Cristina, F. M. Costa, (2003) J. Magn. Magn. Mater., 256, p. 174.

[71] J. G. S. Duquea, E. A. Souzaa, C. T. Menesesa, L. Kubota, (2007) Physica B, 398, p. 287–290.

[72] L. C. R. Nell, (1950) Acad. Sci., Ser. 1 Math., 230, p. 375.

[73] S. Morup., (1994) Superparamagnetism and Spin Glass Ordering in Magnetic Nanocomposites, Europhys. Lett., 28, p. 671–676.

[74] J. Torrent, V. Barron, (2002) Diffuse Reflectance Spectroscopy of Iron Oxides, Encyclopedia of Surface and Colloid Science New York, Marcel Dekker, Inc. p. 1438-1446.